Inherited anthropogenic disturbance and decadal sediment dynamics in a mountain fluvial system: The case of the Marecchia River canyon, Northern Apennines

Inherited anthropogenic disturbance and decadal sediment dynamics in a mountain fluvial system: The case of the Marecchia River canyon, Northern Apennines

Manel Llena[1,†,*], Tommaso Simonelli[2], and Francesco Brardinoni[1,†]
[1]*Department of Biological, Geological and Environmental Sciences, University of Bologna, 40126 Bologna, Italy*
[2]*Autorità di Bacino Distrettuale del Fiume Po, 43121 Parma, Italy*

ABSTRACT

We evaluate decadal coarse sediment dynamics along the Marecchia River of the Northern Apennines, a fluvial system with a history of gravel mining that led to the incision of a 6-km-long canyon. To this purpose, we subdivided the river into 21 reaches, seen as sediment reservoirs, to examine (1) historical variations in active channel width (1955–2019) in conjunction with (2) change in alluvial sediment storage (2009–2019), by differencing two sequential LiDAR digital elevation models (DEMs) within the active channel footprint. Combined examination of lateral (widening or narrowing) and vertical (aggradation or degradation) channel changes allowed the identification of composite styles of reservoir adjustment, as well as the refinement of geomorphic inference solely based on changes in active channel width. In particular, we find that different styles of decadal adjustment (1) are compatible with supply- and transport-limited conditions, as constrained by degree of confinement, stream channel slope, and active channel width; and (2) indicate different stages of evolution at reservoirs located upstream and downstream of the canyon head (dynamic equilibrium vs. transient response). The persistence of this geomorphic divide is supported over historical timescales by distinctive trends in planform channel changes, suggesting that sedimentary signal propagation downstream becomes abruptly interrupted at the canyon head. Over this 10-year natural experiment, the spatial pattern of erosion along the canyon exemplifies a striking case of transient response to anthropogenic forcing, where decadal topographic change, modulated by varying styles of hillslope-channel coupling, declines nonlinearly downstream. Depth of incision along the canyon increases progressively upstream, suggesting that the canyon head has been evolving toward a more unstable configuration with no significant change in sediment supply. This tendency, which points to a possible runaway style of development as bedload wearing on weak pelitic side walls continues, may hold basic implications for our understanding of channel incision into bedrock and strath terrace formation.

1. INTRODUCTION

In a fluvial system, clastic sediment transfer occurs through a series of natural reservoirs (Dietrich et al., 1982; Kelsey et al., 1987; Benda and Dunne, 1997), each of which is characterized by its peculiar ability to store or convey sediment downstream, depending on the rate of supply and the amount of sediment currently stored (Lisle and Church, 2002). Mountain fluvial systems host complex arrays of alluvial reservoirs (e.g., channel reaches) that mediate sediment export from the inner portions of mountain belts out to unconfined forelands and eventually to the sea (Milliman and Syvitski, 1992; Milliman and Farnsworth, 2011). They are transitional environments that typically cross diverse geologic domains with a variety of lithological and structural discontinuities that impose local channel slope, hillslope-channel coupling, and confinement (e.g., Kuo and Brierley, 2013; Toone et al., 2014; Hassan et al., 2019). As such, they may experience variations in sediment supply originating further upstream—for example, an outburst flood, or the development of a landslide dam—or respond to downstream-borne perturbations related to base level fall.

In active tectonic settings, the contribution of mountain fluvial corridors to orogen unloading makes them prominent players in the feedback mechanisms linking subaerial erosion and tectonic uplift (Whipple, 2001; Cyr and Granger, 2008). From a more applied perspective, sediment dynamics of alluvial reservoirs along mountain fluvial corridors affect and have been affected by human activities. On the one hand, as preferential pathways for accessing and bypassing mountain barriers, they have been historical sources of raw material for construction works and consequently have often witnessed dramatic depletion in sediment storage; on the other, the implementation of engineering structures for flood protection, or hydropower production, have largely disconnected fluvial corridors from their natural sinks, inducing local sedimentary disequilibrium and hence adding further complexity to already complex systems. Considering their basic and applied relevance, a quantitative appraisal of how mountain fluvial corridors in the Anthropocene adjust to anthropogenic forcing is critical for understanding inherent transient responses, as well as for ensuring basin-wide, sustainable sediment management.

It has long been acknowledged that a graded stream can accommodate variations in sediment supply by adjusting its characteristics—including gradient, morphology (width, depth, roughness) or bed surface texture—at no excess capacity (e.g., Gilbert, 1914; Mackin, 1948) in a variety of morphological settings (e.g., Leopold and Bull, 1979; Lisle, 1982; Madej, 2001; Cook et al., 2020). But departures from graded responses (i.e., adjustments entailing aggradation or degradation that leads to significant change in storage) have received less attention and are not well understood. This is a critical shortcoming, since change in sediment storage forms a fundamental yet elusive component of

the alluvial sediment budget, which summarizes the (im)balance between sediment input and output in a given reservoir of interest. As such, it represents a key geomorphic variable for evaluating the dynamic state of a fluvial system under a given disturbance regime (Reid and Dunne, 1996; Benda et al., 1998; Slaymaker, 2003) and its likely trajectory of evolution.

For example, excess sediment storage, and the rate at which sediment may be recruited from inherited reservoirs within a landscape, can alter downstream fluvial sediment flux for decades and even up to millennia (Trimble, 1983; Church and Slaymaker, 1989; Brardinoni et al., 2018). Conversely, storage depletion through prolonged reduction of sediment supply (relative to transport capacity) may lead to substrate exposure, trigger local incision into bedrock through bedload saltation (Sklar and Dietrich, 2004), and eventually induce an upstream pulse of vertical lowering. Bedrock incision could then continue until a climate-driven increase in sediment supply armors the bed, favoring lateral planation over vertical incision, with subsequent strath formation (e.g., Gilbert, 1877; Wegmann and Pazzaglia, 2002; Fuller et al., 2009). Today, technological advances in remote acquisition of high-resolution bare topography allows the quantification of change in sediment storage over large fluvial systems through differencing of sequential digital elevation models (DEMs) (Wheaton et al., 2010; Vericat et al., 2017), hence bridging an outstanding historical limitation, i.e., beyond extrapolations drawn from reference channel cross sections.

The Marecchia River in the Northern Apennines, with its composite geological setting and a well-constrained history of anthropogenic disturbance, offers an opportunity to examine the style and pace of decadal evolution of a perturbed fluvial system. Following intense and prolonged gravel mining after World War II, the river underwent dramatic morphological changes along the formerly braided reaches of its piedmont alluvial fan. Since then, the combination of mining-induced base-level fall and bedload wearing on the newly exposed weak lithology (i.e., Pliocene claystones and poorly consolidated fine sands) has led to the incision of a 6-km-long canyon, which today continues to grow headward (Llena et al., 2022).

The high geomorphic activity recorded along the entire fluvial corridor, and the short timescales involved with the development of this canyon, make the Marecchia River a particularly intriguing case for at least two reasons: (1) to understand the ongoing storage adjustment of the reservoirs comprising the Marecchia River corridor, with reference to the position of the canyon; and (2) to directly investigate the transient (non-catastrophic) dynamics of canyon development in a natural laboratory setup, building on prior work that relied on analogue experiments (e.g., Thompson and Wohl, 1998; Cantelli et al., 2004; Finnegan et al., 2007; Lamb et al., 2015), numerical modeling (e.g., Sklar and Dietrich, 1998; Snyder and Whipple, 2003; Yanites, 2018), and reconstructions of paleo-megafloods (e.g., Lamb et al., 2014; Baynes et al., 2015).

Beyond the Marecchia case study, the broader objective of this paper is to shed light on the controls that mediate coarse sediment storage and conveyance in mountain fluvial systems of the Anthropocene, where inherited human disturbance is the main driver of change. In this context, we aim to: (1) investigate, through explicit examination of change in storage, whether and how the style of decadal adjustment of alluvial reservoirs varies beyond gradation along a perturbed fluvial corridor; and (2) characterize the pace and style of canyon incision into bedrock in controlled conditions, i.e., away from negative feedback mechanisms induced by lateral coarse-grained sediment supply (Shobe et al., 2016; Glade et al., 2019).

To pursue these objectives at high spatial resolution, we utilized two LiDAR DEMs acquired in 2009 and 2019. In particular, to track planimetric channel adjustment, after partitioning the main stem of the Marecchia River into morphologically homogeneous reaches (the natural sediment reservoirs), we mapped the active channel bed on LiDAR-derived hillshades and optical imagery acquired in 2009 and 2019 and evaluated variations in active channel width. Concurrently, through differencing of the two LiDAR DEMs on the combined 2009–2019 active channel footprint, we evaluated vertical topographic variations. Outside the canyon, these variations correspond to volumetric changes in alluvial sediment storage, including sediment exchange between the active channel bed and the hosting floodplain (e.g., Dunne et al., 1998). Within the canyon, they constrain rates of waterfall bedrock erosion and valley widening through side wall failures (see section 3 for a description of the methods).

2. SETTING

The study area comprises the 50 km valley segment of the Marecchia River (basin area = 610 km^2), which extends from the confluence with Senatello Creek (375 m above sea level [asl]) down to the confluence with Ausa Creek (5 m asl) (Fig. 1). The river originates from Monte Zucca (1263 m asl) and flows northwest for $\sim$70 km before entering the Adriatic Sea in Rimini, in the Emilia-Romagna region of Italy. With reference to the Koppen-Geiger classification, the climate is temperate (Cfa), with dry and hot summers. Mean annual precipitation (1988–2019) ranges from 703 mm in Rimini (7 m asl) and 766 mm in San Marino (670 m asl) to 1320 mm in Badia Tedalda (756 m asl) (ARPAE, 2019).

The study basin lies within the Val Marecchia Nappe, which is composed of stacked slices of Ligurian and Epiligurian rocks that during the Neogene tectonic phases overrode the Umbria-Marche units and Miocene–Pleistocene successions (Conti et al., 2016). Ligurian units are located in the middle part of the basin and are mainly made of a pelitic basal complex with calcareous and arenaceous intercalations (i.e., the Argille Varicolori, Pugliano, Sillano, and Argille a Palombini formations). Epiligurian units overlie Ligurian units and consist of several depositional sequences that are interrupted by discontinuities and unconformities and mainly composed of reworked marly-arenaceous deposits (Campaolo and Carnaio formations), biogenic limestones (San Marino Formation), mudstones and marls (Barbotto and Montebello formations), as well as conglomerates and sandstones (Acquaviva and Casa Monte Sabatino formations). Underneath the Ligurian units are outcrops of the Umbria-Marche Domain in the upper part of the basin, and Miocene–Pleistocene successions in the mid-to-lower portions, respectively. The Umbria-Marche Domain is mainly composed of mudstones, turbiditic sandstones, and siltstones with interbedded marls (Marnoso-Arenacea Formation). Miocene–Pleistocene successions consist of clays and silty clays interbedded with sandstones and conglomerates (Argille Azzurre Formation) (Tinterri and Muzzi-Magalhaes, 2011; Conti et al., 2016; Conti et al., 2019). Modern rates of uplift (1943–2003) in the Marecchia valley are 0.41 ± 0.26 ($\pm$1 STD) mm/yr (D'Anastasio et al., 2006).

The variety of outcropping lithologies and the history of anthropogenic disturbance locally condition, or have altered, the geometry of the valley floor and the planform pattern of the Marecchia active channel, and therefore its degree of lateral confinement. As a result, today the river flows across wide, unconfined, wandering-to-braided channel reaches (i.e., reaches 2, 9, 11–13, and 18–20) separated by single-thread reaches along natural gorges—such those associated with competent limestones of the San Marino Formation near Ponte Santa Maria (S.M.) Maddalena and Ponte Verucchio (i.e., reaches 10 and 13)—and along the canyon developed over the past 70 years downstream of Ponte Verucchio (i.e., reaches 14 through 17; Figs. 2 and 3A).

After World War II, the Marecchia underwent severe anthropogenic disturbance due to intense and prolonged gravel mining. Conservative

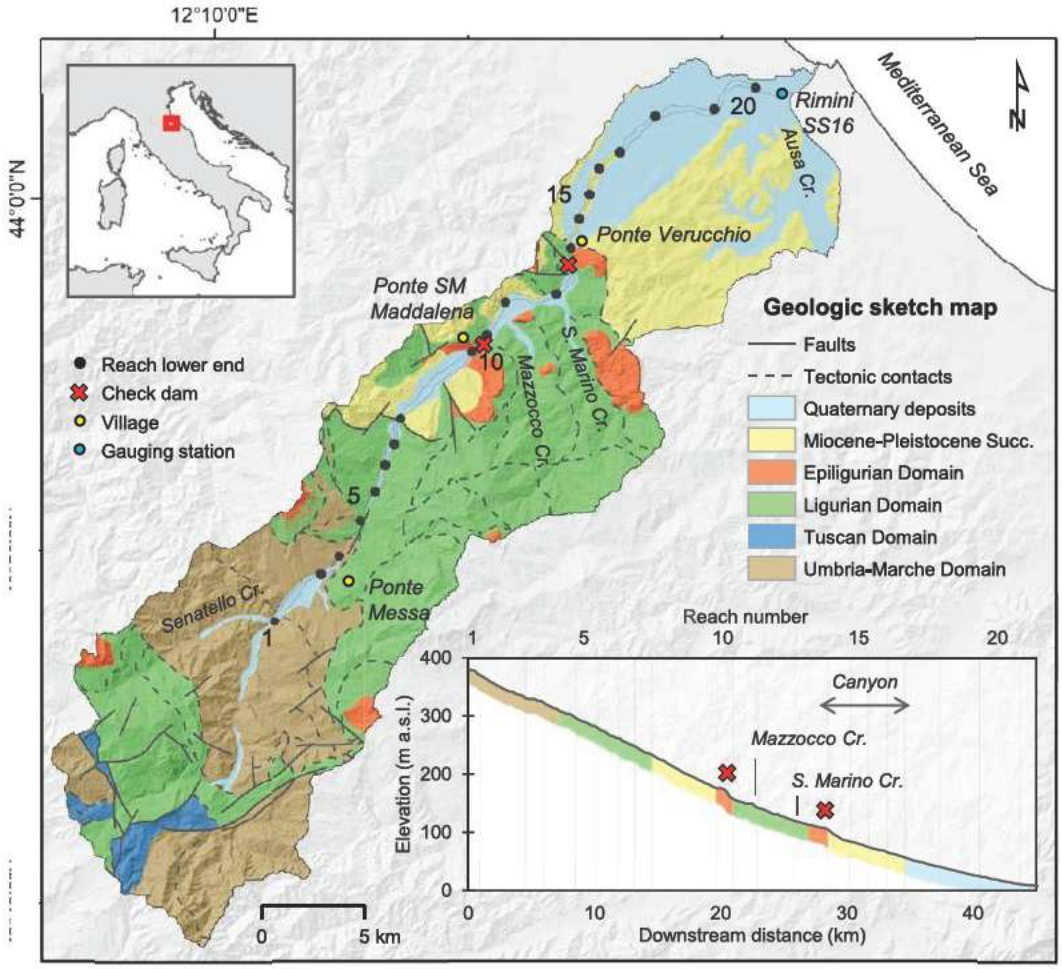

Figure 1. Geologic sketch map showing the study area and the corresponding longitudinal profile of the study segment (simplified after Conti et al., 2016, 2019). Quaternary deposits: mainly alluvial deposits on the main floodplain and on the tributary alluvial fans; Miocene–Pleistocene succession: clays interbedded with sandstones; Epiligurian Domain: marly sandstones, limestones, and conglomerates; Ligurian Domain: pelitic complex with limestones and sandstones; Tuscan Domain: sandstones, marls, and siltstones; Umbria-Marche Domain: mudstones, sandstones, and siltstones. Cr.—creek.

estimates report that between 1950 and 1977, $\sim 13 \cdot 10^6$ m^3 of alluvium was extracted from the distal reaches of the river bed (IDROSER, 1981). Locally, river bed excavation caused abrupt base-level drop and exposed highly erodible mudstone and poorly consolidated sands of the Argille Azzurre Formation (Figs. 1 and 2), promoting rapid vertical incision into bedrock and headward knickpoint migration. Today, this vertical adjustment continues and cumulatively has carved a canyon that is ~6 km long and 10–20 m deep. To prevent bedrock incision from reaching a bridge and secure a stable site for water diversion to irrigation, a major check dam was built in 1987 at Ponte Verucchio (Fig. 1). Other major check dams can be found 500 m upstream of Ponte Verucchio and further away near Ponte S.M. Maddalena (Fig. 2 and Supplemental Material Fig. S1[1]).

[1]Supplemental Material. Composed by 2 tables and 10 figures. Please visit https: // doi .org /10 .1130 / GSAB .S.22557814 to access the supplemental material, and contact editing @ with any geosociety.org questions.

2.1. Hydrology

Flood characterization relies on the 30 min time series recorded between 2006 and 2021 at the Rimini SS16 gauging station (10 m asl; Figs. 1 and 2) of the Regional Agency for Prevention, Environment and Energy (ARPAE). This period is characterized by a mean annual discharge of 5.9 m^3/s, a maximum daily discharge of 814 m^3/s (i.e., 1 February 2009), and a mean annual peak flow of 393 m^3/s. The channel changes captured between the two sequential topographic surveys (i.e., July 2009 and March 2019) integrate the effects of several floods. Four of these, which scored above the 2-yr recurrence interval (405 m^3/s; period 2006–2021), are clustered between 2013 and 2015 (Fig. 2D).

3. DATA COLLECTION AND METHODS

Decadal topographic changes along the Marecchia River corridor are estimated by DEM of difference (DoD) analysis performed on two sequential, 1 m bare-earth, gridded DEMs derived from LiDAR airborne surveys conducted in July 2009 (1.5 points per m^2) and March 2019 (2.5 points per m^2). Root mean square error (RMSE) against GPS elevation points collected on stable (unchanged) topography equals, respectively, 0.087 m in 2009 and 0.078 m in 2019 point clouds. The two DEMs were obtained from each point cloud after filtering for vegetation and noise. Uncertainty on each DEM is evaluated through the application of Fuzzy Inference Systems (FIS), then propagated to the relevant DoD (Wheaton et al., 2010). In particular, we applied a FIS model that considers vertical uncertainty to be a function of point density, slope, roughness, and wetted area. Resulting error surface models range from 0.03 m to 0.50 m, with median values of 0.15 m and 0.06 m associated, respectively, with the 2009 and 2019 DEM. A critical t-value, using a 95% confidence interval, was then applied to these error surfaces to calculate the spatially distributed minimum level of detection (minLoD). Accordingly, DoD cells with absolute values below the minLoD were discarded from the computation of the so-called thresholded DoD.

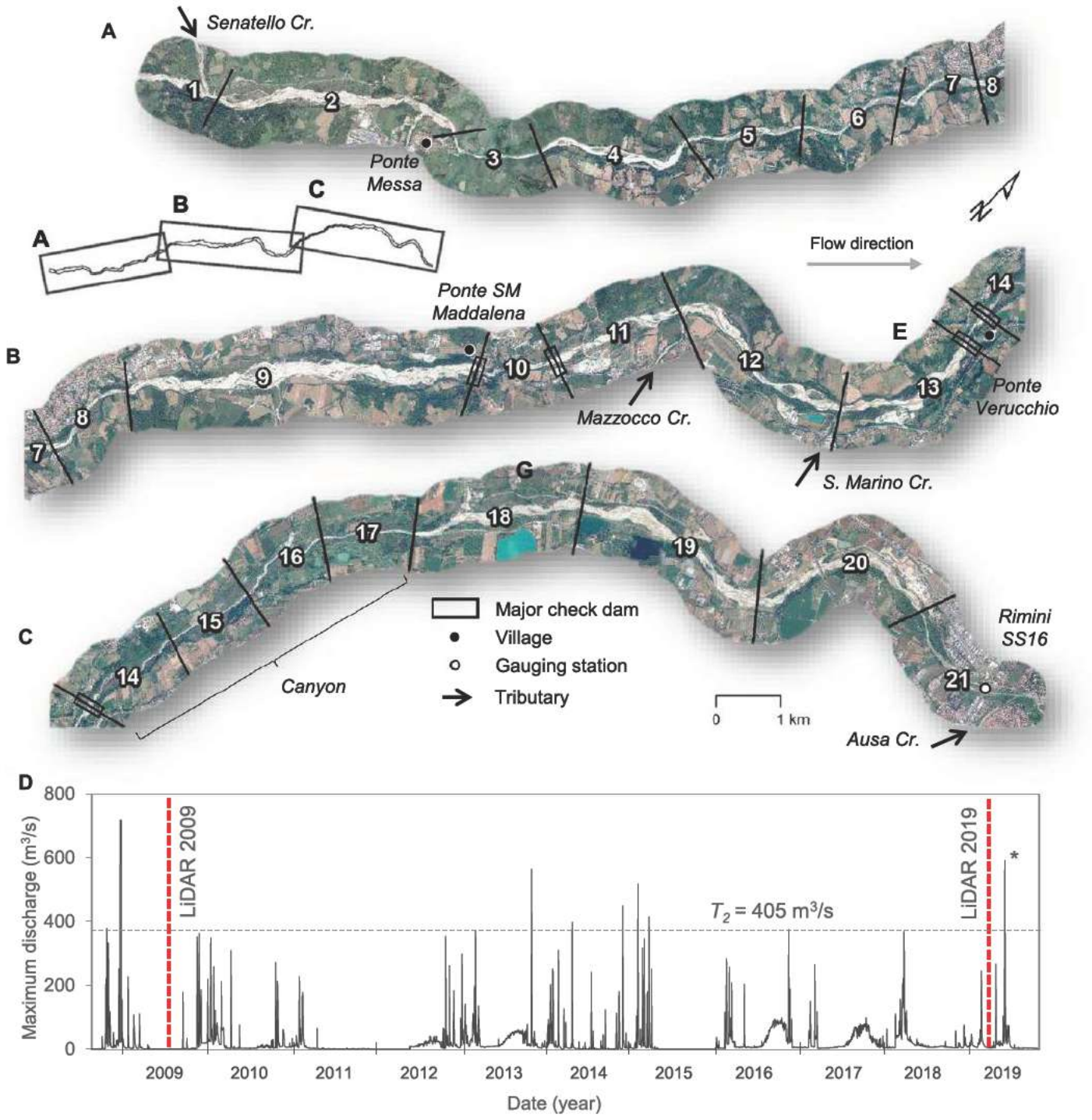

Figure 2. (A–C) Orthophoto mosaics (year 2009) of the Marecchia River valley segmented into 21 study reaches. (D) Maximum daily peak discharge record during the study period measured at Rimini SS16 gauging station (10 m asl). T_2 indicates the 2-yr peak flow. Star indicates the peak flow of 590 m³/s (May 2019) associated with the collapse of the Ponte Verucchio check dam.

The thresholded DoD was applied both at the scale of the entire Marecchia valley segment and at the reach scale, within the combined footprint of the active channel bed (e.g., Surian et al., 2009), as manually mapped on 2009 and 2019 optical ortho-imagery and LiDAR-derived hillshade raster. Active channel width, which includes the low-flow channel and unvegetated or sparsely vegetated bars, has been used as a proxy of reach-based transport capacity in relation to (in-channel) sediment storage and (upstream and lateral) sediment supply (Church, 2006; Bertrand and Liébault, 2019; Brenna et al., 2022). In this work, because wide channels generally evolve where there is a lot of lateral motion due to active bar deposition, we use the active channel width as a qualitative indicator of local coarse

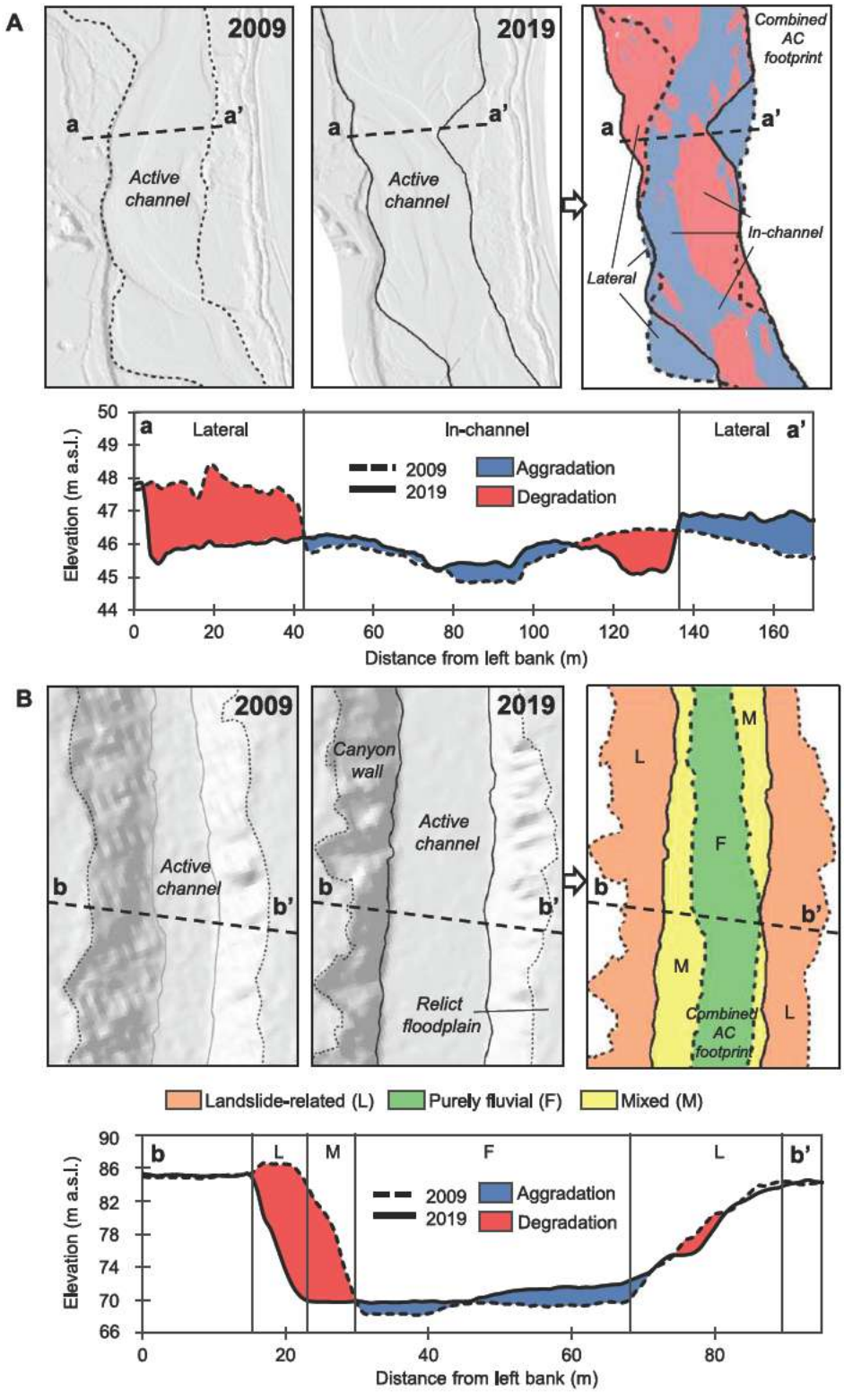

Figure 3. (A) Planimetric and cross-sectional views of a sample channel stretch representing the boundaries of the active channel bed as mapped in 2009 and 2019, and the combined active channel (AC) footprint, together with the spatial partitioning of topographic change (i.e., aggradation and degradation) into in-channel and lateral change in alluvial sediment storage. (B) Planimetric and cross-sectional views of a sample canyon stretch representing the boundaries of the active channel bed (solid lines) and the canyon walls (dotted lines) as mapped in 2009 and 2019, and the combined active channel (AC) footprint, together with the spatial partitioning of topographic change into three geomorphic components: landslide-related (L), purely fluvial (F), and mixed (M). The latter represents a transition zone where landslide footprints (in 2009) and the active channel bed (in 2019) overlap.

sediment deposition (or the divergence of the sediment flux).

To control for the effects of local anomalies associated with discrete water and sediment inputs (e.g., tributary confluences) and barriers (e.g., check dams) that may confound natural spatial patterns of planimetric and vertical channel changes, we subdivided the Marecchia River into 21 morphologically homogeneous reaches (e.g., Grant and Swanson, 1995; Montgomery and Buffington, 1997). Besides accounting for sources of lateral and longitudinal discontinuity, reach delineation was based on planimetric channel pattern, sinuosity, and degree of lateral confinement of the active channel bed. In particular, the reaches' lower ends were set: (1) upstream of major tributary confluences (i.e., Senatello Cr. in reach 1, Mazzocco Cr. in reach 11, and S. Marino Cr. in reach 12); (2) at major check dams (i.e., Ponte S.M. Maddalena in reach 10 and Ponte Verucchio in reach 13); and (3) at transitions between single- and multithread channel stretches, as well as between confined and unconfined ones (e.g., reaches 2, 3, 4, 8, 10, 14, 17, and 20). In channel stretches characterized by consistent channel pattern and confinement, further breaks mark the distinction between sinuous (e.g., reaches 14 and 16) and rectilinear reaches (e.g., reaches 15 and 17). Finally, to avoid morphological over-fragmentation and ensure representativeness over local noise, minimum reach length was set to a threshold of 20 local channel widths (e.g., Montgomery and Buffington, 1997; Brardinoni and Hassan, 2007). This morphological approach aims to minimize within-reach heterogeneity while maximizing between-reach differences, so that channel changes may be evaluated in relation to different channel types.

To aid interpretation of the planimetric changes (i.e., widening or narrowing) observed within the 2009–2019 study period, we increased the resolution of the multi-temporal mapping by outlining active channel width on orthophoto sets taken in 2012, 2014, and 2017. Most importantly, to define the historical context of fluvial

adjustment in which the 2009–2019 period is nested, we mapped active channel width on seven additional orthophoto sets (i.e., photo years 1955, 1969, 1976, 1985, 1996, 2000, and 2006). Finally, to gain additional understanding of historical channel changes that were otherwise solely based on variations in active channel width, we exploited two sets of cross-sectional surveys conducted in 1994 (n = 48) and 1999 (n = 83). The former spans from kilometer 30 to kilometer 50, across the mid to lower portions of the valley segment; the latter spans from metric distance 0 to kilometer 30, in the upper course of the river (Fig. S2; see footnote 1). As will become clear in sections 4 and 5, combining these sets of information allowed clarifying correspondence between planimetric and vertical channel changes after 1994 (e.g., whether or not widening meant bed aggradation, and narrowing meant bed degradation).

To account for lateral migration potential, the degree of channel confinement was estimated at the reach scale, where confinement is expressed in percent form as the ratio between the length of the active channel margins (i.e., the banks) that run along a confining edge (e.g., a hillslope, a terrace, a tributary fan, or a dike) and the total length of the channel banks (Fryirs et al., 2016; O'Brien et al., 2019), including those bounding the modern alluvial floodplain, where resistance to lateral migration is lowest (Fig. S3). To provide a first-order assessment of available energy, local slope (e.g., Hickey et al., 1994) and a specific stream-power index (e.g., Brummer and Montgomery, 2003; Dell'Agnese et al., 2015) were calculated at the reach scale. To explore possible interrelations among "initial" channel-reach characteristics as imaged by the 2009 LiDAR survey, we conducted Pearson's linear correlation testing across the 21 study reaches.

Reach-based volumetric variables associated with topographic change restricted to the combined 2009–2019 active channel footprint include: aggradation as surface rising, degradation as surface lowering, gross change as the sum of aggradation and degradation, and net change as the difference between aggradation and degradation. The latter represents the change in alluvial storage, a fundamental component of the alluvial sediment budget that summarizes the (im)balance between sediment input and output in a given reach.

The combination of multitemporal planimetric mapping and sequential differencing of high-resolution DEMs allows for the partitioning of changes in alluvial storage into *in-channel* and *lateral* components (Fig. 3A). The former accounts for volumetric changes in alluvial storage recorded within polygons where active channel footprints, as mapped in 2009 and 2019, overlap. The latter refers to counterparts associated with lateral migration dynamics, including sediment exchange (recruitment and sequestration) between the active channel bed and the hosting floodplain (Dunne et al., 1998).

Within the canyon, this classification scheme for change in alluvial storage does not apply since channel-lateral migration involves direct interaction with the adjoining bedrock walls (as opposed to alluvial deposits of the modern floodplain) and widespread landslide activity. To evaluate the contribution of landsliding to the canyon sediment budget, and the significance of hillslope-channel coupling (Brunsden and Thornes, 1979; Caine and Swanson, 1989) to the evolution of canyon geometry, in reaches 14 through 17, we mapped rotational landslides and canyon-wall collapses on aerial photos and LiDAR-derived hillshades acquired between 2009 and 2019, as well as the top margins of the canyon walls in 2009 and 2019 (Fig. 3B). The latter set of margins bounds our area of interest.

Subsequently, based on the topological relations between the 2009 and 2019 mapped geomorphic features (i.e., polygon outlines of landslide scars, canyon walls, and active channel beds), we partitioned thresholded volumetric changes into three main components: (1) landslide-related; (2) purely fluvial; and (3) mixed (Fig. 3B). The first refers to volumetric changes computed within new landslide polygons identified in 2019. The second accounts for changes recorded within polygons where active channel footprints, as mapped in 2009 and 2019, overlap. The third refers to changes that occurred within the 2009 canyon walls (including margins of the relict Marecchia floodplain) that by 2019 had become part of the active channel bed, due to the combined activity of river lateral migration, slope undercutting, and canyon-wall failure (Fig. 3B).

4. RESULTS

We begin by providing historical context to the 2009–2019 study period and illustrate planimetric channel adjustment across the main valley segments (Fig. 4), which we interpret by integrating channel cross sections surveyed in 1994 and 1999 (Fig. 5). We continue by presenting and analyzing initial channel-reach characteristics from 2009. These include channel pattern, median slope gradient, confinement, active channel width (ACW), and a specific stream-power index (SSPI) (Table 1 and Figs. 6A and 7), as derived from the first LiDAR survey in July 2009. We then examine 2009–2019 planimetric variations in active channel width (Fig. 6B), in conjunction with reach-based volumetric changes in sediment storage (i.e., net topographic change within the active channel bed footprint) derived from thresholded DoD analysis (Figs. 6C and S4; see footnote 1). We further distinguish in-channel changes in storage from those associated with lateral migration dynamics (Fig. 8), and evaluate their significance in the context of the combined, valley scale budget (Fig. 9).

To address the objectives of this paper, in presenting the results, consideration will be given to the dynamics of canyon evolution (reaches 14 through 17; section 4.3) and to possible disturbance that this may bring to the main alluvial sediment stores located upstream (reaches 11, 12, and 13) and downstream (reaches 18, 19, and 20). In this context, reach 2 (the "headmost" large alluvial store, which we label "Control 1") and reach 9 ("Control 2") are regarded as undisturbed references, since—in principle—they are disconnected from possible canyon-borne perturbations by the natural gorge of Ponte S.M. Maddalena in reach 10 (Figs. 1 and 2). Disconnection is promoted by the two check dams located, respectively, at the entrance and exit of the gorge, and by massive boulder-cascades that characterize this channel reach. We conclude by focusing on the 2009–2019 topographic and geometric changes associated with the evolution of the Marecchia River canyon (Fig. 10).

4.1. Historical Context of Channel Adjustment

Planform channel changes of the Marecchia River between 2009 and 2019 are nested in a broader historical trajectory that has seen substantial channel narrowing in the second half of the 20th century—roughly until photo year 1996—followed by slow and ongoing recovery to wider channel configurations (Fig. 4). Historical planimetric evolution of five strategic valley segments displays variability both before and after 1996 (Fig. 4), suggesting diverse styles of channel adjustment along the study corridor. Post-1955 cumulative narrowing, in a phase of generalized channel incision (cf. level of 1955 active channel bed in selected cross sections; Fig. 5), varies from 48% to 50% in the two control segments, where channel pattern has remained braided through the decades, to 66% and 65% in the wandering segments located respectively upstream and downstream of the canyon, and up to 93% in the formerly braiding reaches of the piedmont fan, which is now replaced by the single-thread channel flowing through the canyon (Fig. 5C; Llena et al., 2022). After 1996, progressive rewidening is observed along the upstream (14%), canyon (6%), and downstream (15%) reservoirs, whereas fluctuations in the two control reservoirs have nearly cancelled out in the past 25 years (Fig. 4). In this context, the canyon behavior differs from the rest

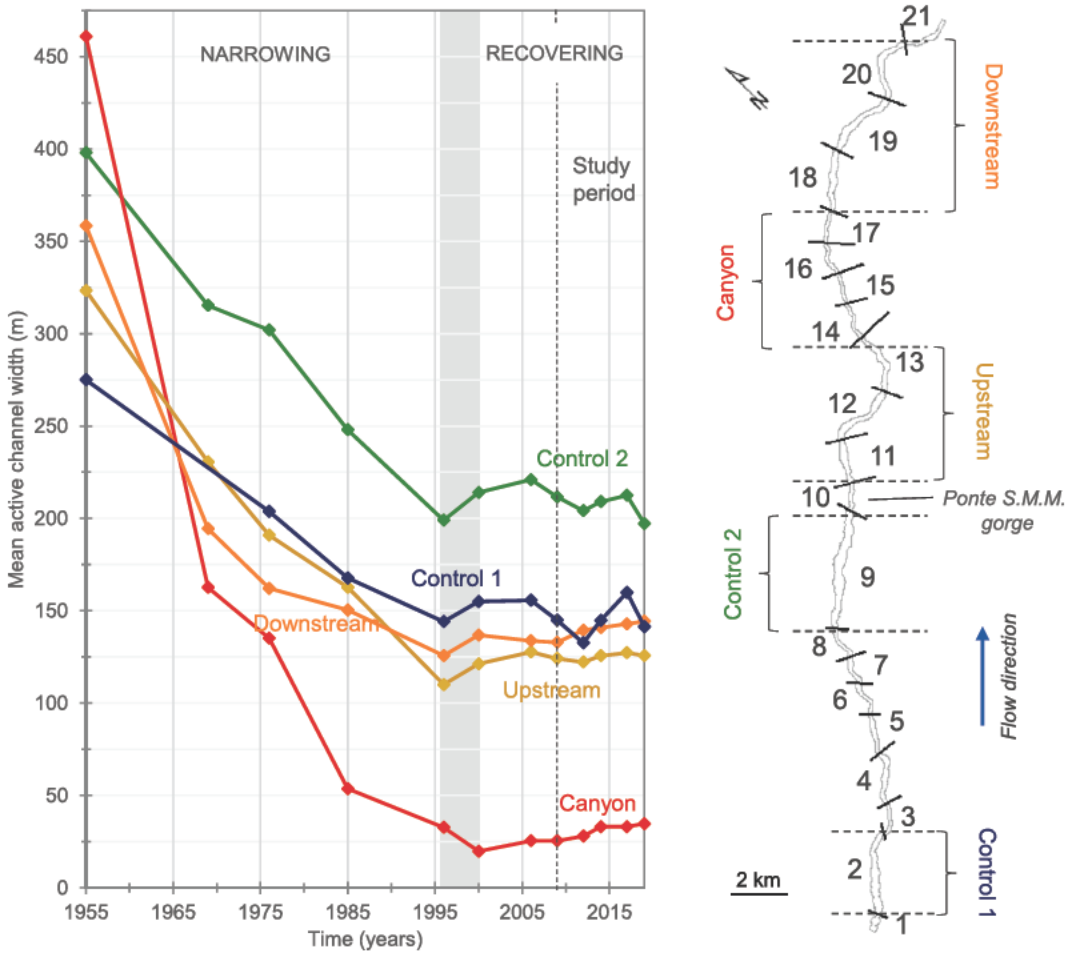

Figure 4. Evolution of active channel width in the Control 1 (reach 2), Control 2 (reach 9), Upstream (reaches 11–13), Canyon (reaches 14–17), and Downstream (reaches 18–20) valley segments between 1955 and 2019. Note that minimum channel width in the canyon is attained in photo year 2000, four years later than in the other valley segments. Ponte S.M.M. gorge—Ponte S.M. Maddalena gorge.

since minimum channel width is attained four years later. This inflection point indicates that, at the segment scale, rates of incision continue to override those associated with canyon widening until photo year 2000, as exemplified in the sample cross section (Fig. 5C).

This pattern of post-disturbance lateral adjustment, here illustrated in sample channel cross sections, manifests along the canyon through vertical incision into weak pelitic bedrock and subsequent landsliding on the canyon walls (Fig. 5C), which supply large amounts of fine material to the Marecchia River (i.e., clay to fine sand; Fig. S1C). Upstream and downstream of the canyon, widening is associated with channel-lateral migration and occurs through bank erosion induced by progradation of channel bars and related flow divergence (Fig. 5D).

4.2. Initial Channel Characteristics

At the time of first LiDAR acquisition, which in this work sets the initial boundary conditions of the study reaches, we observe high variability in active channel width, with wide alluvial sediment stores (i.e., ACW >125 m in reaches 2, 9, 11–13, and 18–20) that alternate to narrow, bedrock-controlled reaches (i.e., ACW <50 m in reaches 3 and 10) and even narrower ones along the anthropogenic-induced canyon (i.e., ACW <35 m in reaches 14 through 17; Fig. 6A and Table 1). This variability is also reflected in median channel slope, stream power, and confinement, in that narrow single-thread reaches display high median slope (hence stream power) and confinement (cf. valley width and active channel width in reaches 14 through 17 along the canyon; Fig. 6A and Table 1), as opposed to wide, braided counterparts. When considering all study reaches, we observe high linear correlations among width, slope, and confinement (Fig. 7). Active channel width decreases as median channel slope (Fig. 7A) and confinement (Fig. 7B) increase; consequently, confinement increases directly with median channel slope (Fig. 7C).

4.3. Decadal Planimetric and Volumetric Channel Changes

Decadal planimetric channel changes depict an upper Marecchia River (i.e., reaches 1–12) largely characterized by narrowing dynamics, and a lower course (i.e., reaches 13–21) where widening dominates (Fig. 6B). Substantial reduction in active channel width (i.e., > 14 m) is focused on reach 2, and on reaches 5 through 9, characterized by varying degrees of confinement (i.e., from 3% to 45%; Table 1) and median slope ranging between 0.055 m/m and 0.080 m/m. In this narrowing context, the 4 m widening at reach 10 (i.e., confinement of 39% and median slope of 0.117 m/m) is associated with the collapse of the Ponte S.M. Maddalena check dam in 2014.

An increase in active channel width occurs both in wide, braided reaches (i.e., reaches 13 and 19 through 21) and across the steep, narrow, and highly confined reaches of the canyon (i.e., reaches 14 through 17; Fig. 6B). In particular, widening dynamics is highest upstream of the canyon (i.e., > 17 m), declines along the canyon (i.e., from 13 m down to 4 m), and reverses to narrowing in reach 18, at the exit of the canyon. Further downstream, widening resumes at reach 19 (i.e., > 26 m) and progressively declines again down to the confluence with Ausa Creek. Overall, changes in active channel width correlate poorly with confinement ($\rho = 0.26$)

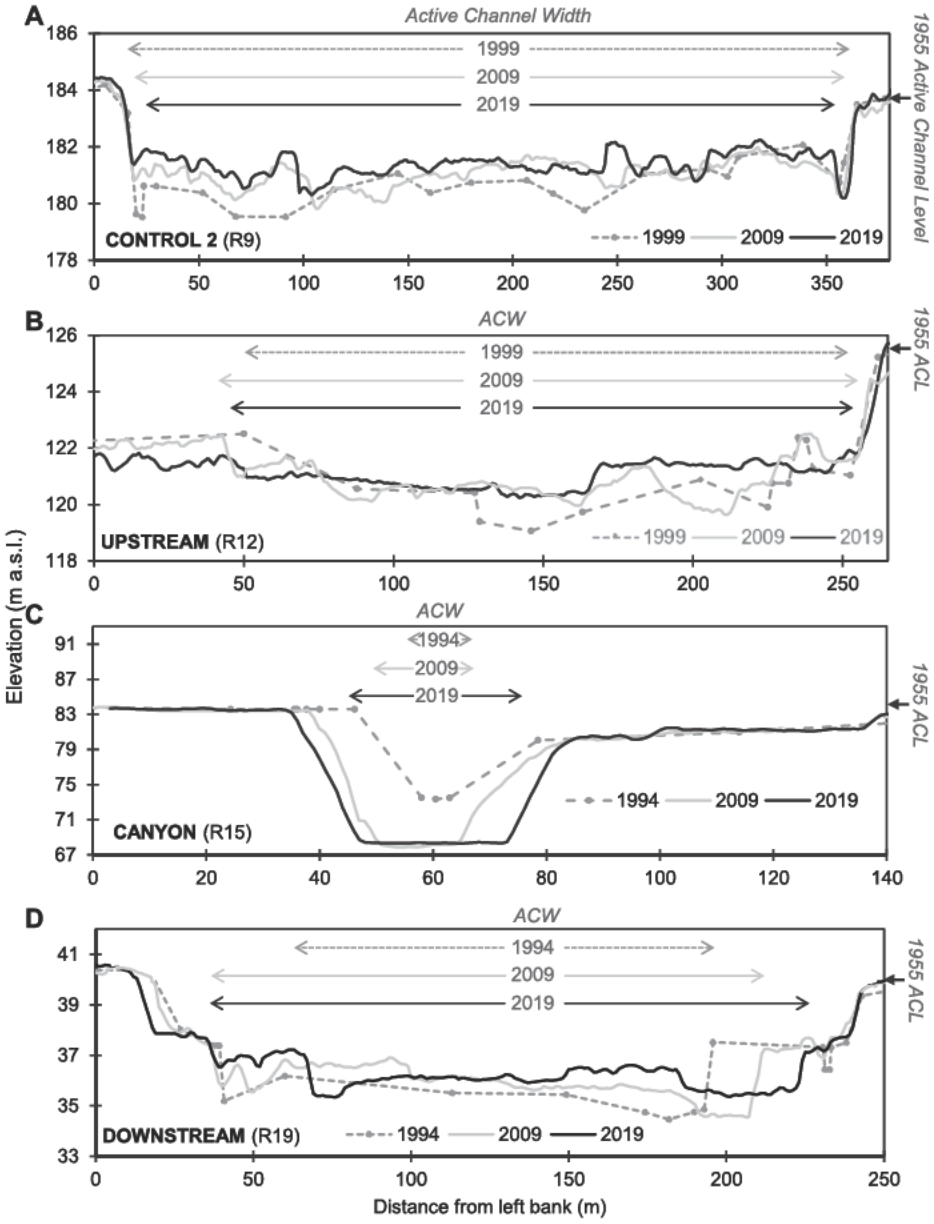

Figure 5. Cross sections illustrating vertical channel changes with reference to the level of the active channel bed in 1955 (i.e., 1955 ACL), and post-1996 adjustment of active channel width (ACW) at representative locations within the reference valley segments: (A) Control 2 (reach 9); (B) Upstream (reach 12); (C) Canyon (reach 15); and (D) Downstream (reach 19). (A) Channel cross section in reach 9 shows bed aggradation and narrowing since 1999. (B) Channel cross section in reach 12 shows progressive main channel aggradation and a left bank lateral degradation in a context of initial widening (1996–2009), followed by narrowing (2009–2019). (C) Reach 15 images dominant incision dynamics between 1994 and 2009, with distinctive transition to valley widening after 2009 via canyon wall retreat. (D) In reach 19, we observe marked dynamics of channel-lateral migration, with erosion of the right channel bank partly offset by aggradation on the opposite side, in a general vertical trend of aggradation and active channel widening.

and median slope ($\rho = 0.30$; scatterplots are not shown).

The spatial distribution of volumetric changes in storage (i.e., aggradation, degradation, and the resulting net change) along the study reaches exhibits both differences from and similarities to changes observed in active channel width (cf. Figs. 6B and 6C). In the upper course (i.e., reaches 1–12), which is dominated by channel narrowing (Fig. 6B), we observe general volumetric balance, with magnitudes of aggradation (blue bars) and degradation (red bars) increasing as a function of reach area (Fig. 6C). In this context, significant departures from balance are observed along the wide, braided reaches 2 and 9, where respectively 180,870 m^3 (+/−40,440 m^3) and 378,840 m^3 (+/−68,490 m^3) of aggradation are recorded (Table S1; see footnote 1). The lower course of the river, where widening is widespread (Fig. 6B), may be broadly subdivided into two parts: reaches 13–17 are characterized by intense net fluvial degradation (i.e., note the one order-of-magnitude decline in degradation along the canyon: from 519,720 m^3 +/−37,770 m^3–24,910 m^3 +/−11,150 m^3), whereas net aggradation prevails in reaches 18–20 (i.e., net volume gain ranges between 13,970 m^3 +/−53,210 m^3 and 81,950 m^3 +/−45,540 m^3; Table S1). Similar to what is observed in reaches 2, 9, 11, and 12, this increase in alluvial storage is associated with high magnitudes of coexisting aggradation and degradation across wide, braided to wandering reaches.

Qualitatively, the combined planimetric representation of channel-bed lateral and vertical changes (i.e., DoD maps of reaches 2, 9, 12–13, and 19–20; Fig. 8) helps clarify that simultaneous high aggradation and degradation magnitudes derive from a mosaic of patches associated with dynamics of in-channel bar migration and channel-lateral migration (including bank erosion), as indicated by erosional patches running along the margins of the active channel. This spatial pattern is common among DoD maps of wide, unconfined reaches located in the upper portion of the river corridor (i.e., reaches 2 and 9; Figs. 8A and 8B), as well as in those located either upstream (i.e., reach 12; Fig. 8C) or downstream (reaches 19 and 20 in Fig. 8D) of the canyon.

Quantitatively, erosional patches associated with bed lateral migration involved 29% of total bank length in reach 2 (i.e., 7 patches), 33% in reach 9 (i.e., 15 patches), and 22% in reach 12 (i.e., 6 patches). These figures grow downstream of the canyon to, respectively, 56% in reach 19 (i.e., 11 patches) and 47% in reach 20 (i.e., 13 patches), suggesting increased lateral instability. In this context, the markedly steeper reach 13 stands out, for it displays large and relatively deep erosional bands both in the central and marginal portions of the active channel (i.e., 9 erosional patches involve 57% of total bank length), which lead to a strongly negative change in storage (Fig. 8C). We ascribe this deficit to the breaching of a check dam located at the downstream end of the reach that was observed between photo years 2003 and 2007.

TABLE 1. INITIAL CHANNEL-REACH CHARACTERISTICS

Reach	Area (ha)	Channel width (m)	Valley width (m)	Confinement (%)	Median slope (m/m)	SSPI (km)	Channel type
1	9.76	84	187	12	0.082	2.01	W
2	67.46	145	296	17	0.064	1.67	B
3	6.74	45	66	45	0.097	5.07	S
4	25.63	85	128	16	0.093	3.40	W
5	15.12	75	160	12	0.078	3.55	W
6	12.49	70	99	42	0.073	4.47	S
7	10.41	76	173	36	0.076	4.73	S
8	9.62	65	185	31	0.080	4.33	S
9	131.90	211	368	3	0.055	1.72	B
10	6.72	45	66	39	0.117	11.77	S
11	30.69	125	222	36	0.061	2.30	W
12	48.01	134	199	19	0.075	2.10	W
13	33.13	113	213	9	0.084	2.66	W
14	3.51	17	21	69	0.120	16.70	S*
15	24.70	22	29	84	0.141	11.71	S*
16	18.36	29	33	62	0.126	8.71	S*
17	22.21	34	45	39	0.094	4.29	S*
18	19.88	152	283	13	0.057	1.80	W
19	71.07	143	268	6	0.051	1.99	W
20	59.87	104	237	13	0.059	2.32	W
21	42.46	41	155	35	0.082	3.04	S

Notes: SSPI—specific stream-power index; W—wandering; B—braided, S—single thread.
*Bedrock channel.

Quantitative decomposition of volumetric changes in "lateral" and "in-channel" components (see Fig. 3A and accompanying text for definitions) reveals that channel migration typically leads to negative changes in alluvial storage (i.e., in 15 out of 21 reaches; Fig. 8E), and that net aggradation tends to dominate the decadal budget at in-channel locations (i.e., in 14 out of 21 reaches). This pattern is observed within the main alluvial sediment stores (i.e., reaches 2, 11, 12, 18, 19, and 20), except in reach 9, where positive change in storage characterizes both in-channel and lateral decadal dynamics, and in reach 13, where net degradation occurs. As expected, all reaches within the actively eroding canyon yield negative net changes with respect to both in-channel and lateral components, with the latter accounting for most of the volumetric alluvial change (i.e., height of red-and-white hatched bars).

When volumetric changes are standardized by reach area, bed aggradation becomes more evenly distributed across reaches (i.e., median = 0.21 m^3/m^2; cf. Figs. 6C and S4 and Table S1). In particular, aggradation at reaches 2 and 9 becomes comparable to that of the neighboring reservoirs, and consequently, the highest specific rates of deposition become those recorded downstream of the canyon, in reaches 19 (0.34 m^3/m^2) and 20 (0.53 m^3/m^2). By contrast, area-based standardization enhances specific rates of erosion along the steepest and most confined reaches. Accordingly, degradation, mainly associated with check dam collapse at reach 10, becomes apparent (0.75 m^3/m^2), and intense degradation at reach 13 (–0.73 m^3/m^2) and across the canyon (i.e., ranges from −0.26 in reach 17 to −2.25 m^3/m^2 in reach 14) is confirmed (Table S1).

Collectively, within the 21 study reaches, the combined area occupied by topographic changes above the minimum level of detection (i.e., median value of 0.15 m) accounts for ∼60% (i.e., 4.07 km^2) of the merged 2009–2019 active channel footprint. Of this surface, 60% is associated with aggradation and the remaining 40% with degradation (Fig. 9A). In volumetric terms, partition of the gross decadal budget (i.e., 4,400,840 m^3) is reversed, with degradation (i.e., 2,516,140 m^3 +/−372,130 m^3 dominating (i.e., 57%) over aggradation (i.e., 1,884,700 m^3 +/−366,180 m^3), and yielding a net negative balance of −631,440 m^3 (Fig. 9B). This area–volume mismatch is mainly due to the tail of the degradation frequency distribution being skewed toward high depths (i.e., > 3 m and up to over 16 m) as opposed to aggradation, where most of the vertical changes involve depths <2 m (Fig. 9B).

4.4. Canyon Evolution

In this section, we focus on the topographic changes recorded along the canyon, expanding the area of DoD analysis outward—beyond the combined footprint of the 2009 and 2019 active channel bed—up to the top margins of the canyon walls as imaged on the 2019 LiDAR-derived DEM. This expansion will allow evaluating the contribution of landsliding to canyon development.

Along the canyon, degradation dominates over aggradation (Fig. 6), with the latter becoming progressively more important moving downstream from reach 14 (6%) through reach 17 (34%) (Fig. 10). During the study period, the main knickpoint migrated upstream for ∼500 m through waterfall-bedrock wearing, whereas the long profile downstream of reach 14 shows relatively minor vertical change (Fig. 10A). This mechanism, which has involved average vertical incision of ∼10 m (Fig. 10A), may be regarded as the main process responsible for the highest rates of channel bed lowering within the proximal portion of reach 14 (Fig. 6). By early March 2019, when the second LiDAR survey took place, knickpoint migration had reached the base of Ponte Verucchio check dam, which at the time displayed severe signs of instability due to undercutting. The structure eventually collapsed on 13 May 2019 during a flood that reached a peak flow of 590 m^3/s (Fig. 2D).

At a qualitative level, downstream of the "headward migration zone," the spatial distribution of erosion involves the entire surface of both valley sides in reaches 14 and 15, regardless of sinuosity. Erosion is focused on the outer margins of meander bends in reach 16 and becomes rare along the rather rectilinear reach 17 (Fig. 10B). The spatial distribution of aggradation along the entire canyon is more discontinuous, except for a 250 m stretch in reach 14, downstream of the headward migration zone. Further downstream, aggradation occurs mainly along the active channel bed and appears to be tightly related to the spatial distribution of degradation patches. In particular, aggradation mainly consists of point bars in the more sinuous stretches (i.e., parts of reach 14 and 16), and lateral bars in more rectilinear ones (i.e., reach 17), alternating to landslide scars or to other erosional features. Aggradation patches observed outside of the active channel footprints (i.e., 2009 and 2019) are associated with the deposition zones of rotational landslides at the base of the canyon walls. Examples of landslide types and hillslope-channel coupling are shown in Figure 11.

To gain additional insights into degrading canyon dynamics beyond the reach scale (Fig. 6) and assess the significance of hillslope-channel coupling on the evolution of canyon geometry, we examined planimetric and volumetric changes at higher spatial resolution. In particular, after subdividing the canyon (i.e., 6250 m in total) into 25 250-m-long segments and following the classification scheme illustrated in Figure 3, we examined volumetric changes of the landslide-related, purely fluvial, and mixed components (Figs. 10 and 12). In planimetric terms, we examined changes in top valley width (i.e., orthogonal distance between the top of the two canyon walls) and active channel width across 250 m channel stretches (Fig. 12A).

In planimetric terms, intra-reach segmentation shows that the highest decadal widening, both in

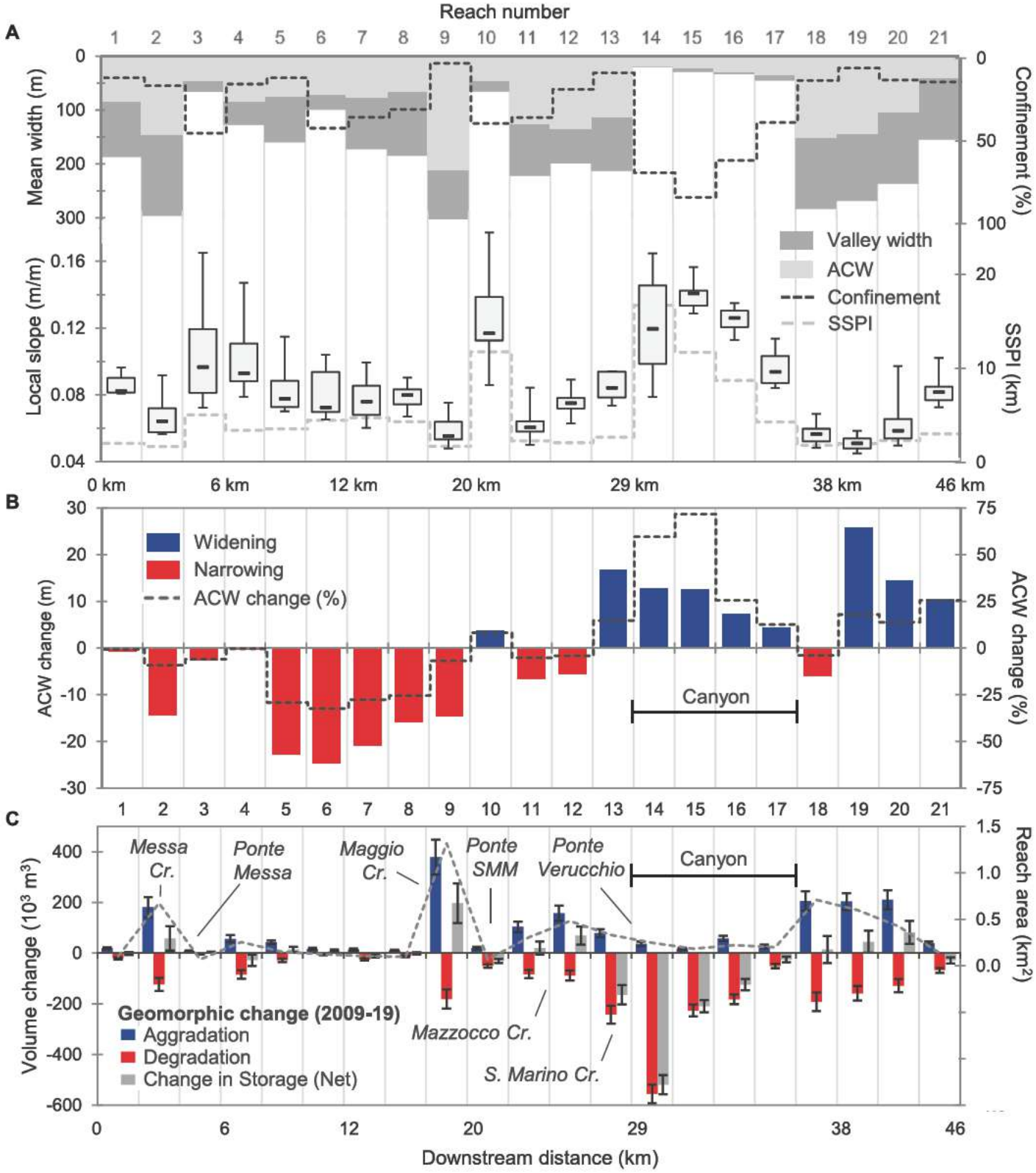

Figure 6. Reach-based spatial variability of: (A) mean active channel width (ACW), valley width, channel confinement, active channel slope (boxplots), and specific stream-power index (SSPI) in 2009; (B) absolute and percent changes in active channel width (ACW) recorded between 2009 and 2019; (C) 2009–2019 volume change associated with bed aggradation, degradation, and the resulting net variation. In panel A, the dash within the interquartile range (the boxes) indicates the reach median slope; whiskers enclose the 10th and 90th slope percentiles. In panel C, dashed linework represents the planimetric area of the reach. Cr.—Creek; Ponte SMM—Ponte S.M. Maddalena.

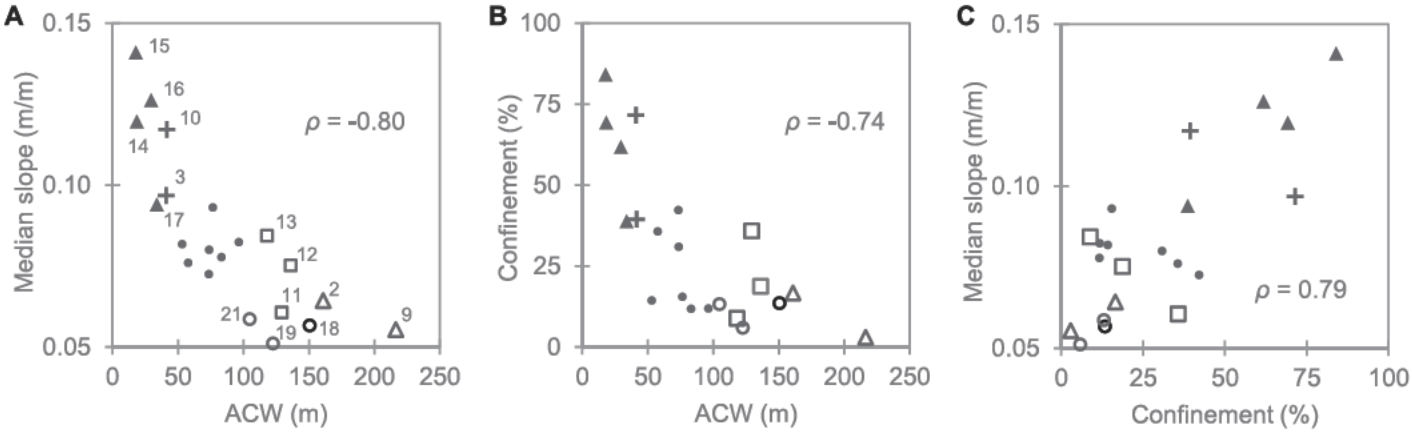

Figure 7. Reach-based scatterplots showing active channel width (ACW) as a function of (A) median slope, (B) confinement, and (C) confinement as a function of median slope. Solid triangles indicate the single-thread, entrenched reaches of the canyon. Large, braided-to-wandering alluvial sediment stores are marked as: empty triangles (control reaches 2 and 9); empty squares (reaches 11, 12, and 13; upstream of the canyon); and empty black circles (reaches 18, 19, and 20; downstream of the canyon). Crosses identify the confined reaches of Ponte Messa (reach 3) and Ponte S.M. Maddalena (reach 10). In panel A, numbers mark reach identification numbers. ρ values indicate Pearson's linear correlation coefficients.

top valley width (i.e., 35 m) and active channel width (i.e., 29 m) occurs by the check dam, in the headmost 250 m of the canyon (Fig. 12A). In the next channel stretch, we observe active channel narrowing (i.e., ∼5 m) and concurrent valley widening (i.e., 7 m) associated, respectively, with intense fluvial channel incision, knickpoint migration, and destabilization of the adjoining canyon walls. Further downstream and down to kilometer 33 in reach 16, top valley widening ranges between 7 m and 20 m, whereas the active channel changes less and widens between 10 m and 17 m. In this context, the discontinuity observed at kilometer 32.25 is associated with stabilization works on the right valley wall. Locally, these operations have induced top valley narrowing (i.e., 10 m) while leaving active channel width unchanged. Downstream of kilometer 33, decadal increase of both top valley and active channel width declines, ranging between 1 m and 11 m (Fig. 12A).

Volumetric intra-reach segmentation confirms intense dynamics of vertical and lateral incision in the headmost half of reach 14 (Figs. 12B, 12C, and 12D). The landslide and mixed components depict similar downstream patterns of volumetric degradation and aggradation along the canyon (Figs. 12B and 12C). Degradation decreases steadily downstream, ranging from 65,730 m^3 (+/−3290 m^3) and 74,410 m^3 (+/−2850 m^3) to 2700 m^3 (+/−390 m^3) and 860 m^3 (+/−130 m^3) for the landslide-related and mixed components, respectively. On the contrary, aggradation is more evenly distributed, except for the abrupt man-made increase in sediment storage at kilometer 32.25 (Figs. 12B and 12C). This anomaly, previously noted in planimetric terms, is observed both in terms of landslide (i.e., 9220 m^3 +/−710 m^3) and mixed (i.e., 11,970 m^3 +/−830 m^3) contributions, which locally make up, respectively, 42% and 55% of the total aggradation recorded in this 250 m stretch (Fig. 12E). Degradation associated with the purely fluvial component mainly occurs in the headmost three segments (Fig. 12D), where it accounts, respectively, for 23%, 51%, and 17% of total degradation. In turn, fluvial aggradation takes place primarily: (1) in three segments located between kilometer 29.5 and kilometer 30.25, where it represents up to 78% (i.e., 5570 m^3 +/−660 m^3) of total aggradation; and (2) downstream of kilometer 32.5, where the fluvial component gains increasing relative importance (i.e., in seven stretches, aggradation accounts for more than 50%; Figs. 12D and 12E).

Overall, decadal volumetric degradation (967,510 m^3 +/−91,910 m^3) is primarily associated with the landslide-related (50%) and the mixed (40%) components, with the purely fluvial counterpart accounting for just 10% (Fig. 12E). By contrast, decadal aggradation (88,100 m^3 +/−8720) displays a more balanced pool of contributions, including: 40% associated with landslides, 38% with fluvial processes, and 22% with the mixed component (Fig. 12E). Cumulatively, degradation operated by the landslides and mixed components increases in nonlinear fashion, as opposed to depositional counterparts that follow a linear growth. Cumulative fluvial aggradation is mostly irregular, with frequent oscillations, and contrasts with fluvial degradation, which is essentially restricted to the first two channel stretches.

5. DISCUSSION

5.1. Characteristic Styles of Adjustment across Natural Sediment Reservoirs

The historical trend of generalized channel narrowing (1955–1996), followed by partial re-widening (1996–2019; Fig. 4), broadly agrees with prior findings and conceptualizations regarding the recent adjustment of European rivers (e.g., Liébault and Piégay, 2001, 2002; Surian and Rinaldi, 2003; Keesstra et al., 2005; Surian et al., 2009; Comiti, 2012; Bollati et al., 2014; Llena et al., 2020; Scorpio and Piegay, 2021). Average channel width reduction by ∼50% was documented between the 1950s and early 1990s in the piedmont, mountain, and small mountain streams of southeastern France (Liébault and Piégay, 2002), as well as in large rivers across Italy (Surian and Rinaldi, 2003). In the former case, reasons were chiefly attributed to land-use changes on floodplains and reduced bedload transport in mountain tributaries due to hillslope afforestation. In Italy, similar reductions in active channel width—paralleled by mean channel incision of 3–4 m (up to 10 m at fixed cross sections) and a shift in channel pattern—were mainly related to gravel mining, dam construction, and channelization. To avoid possible confounding associated with varying degree of (natural or anthropogenic) confinement, more recent comparative studies have rightly focused on unconfined lowland rivers and selected unconfined reaches of mountain systems. In some of these cases, depending on initial morphologic conditions, active channel widths between the 1950s and 1990s were found

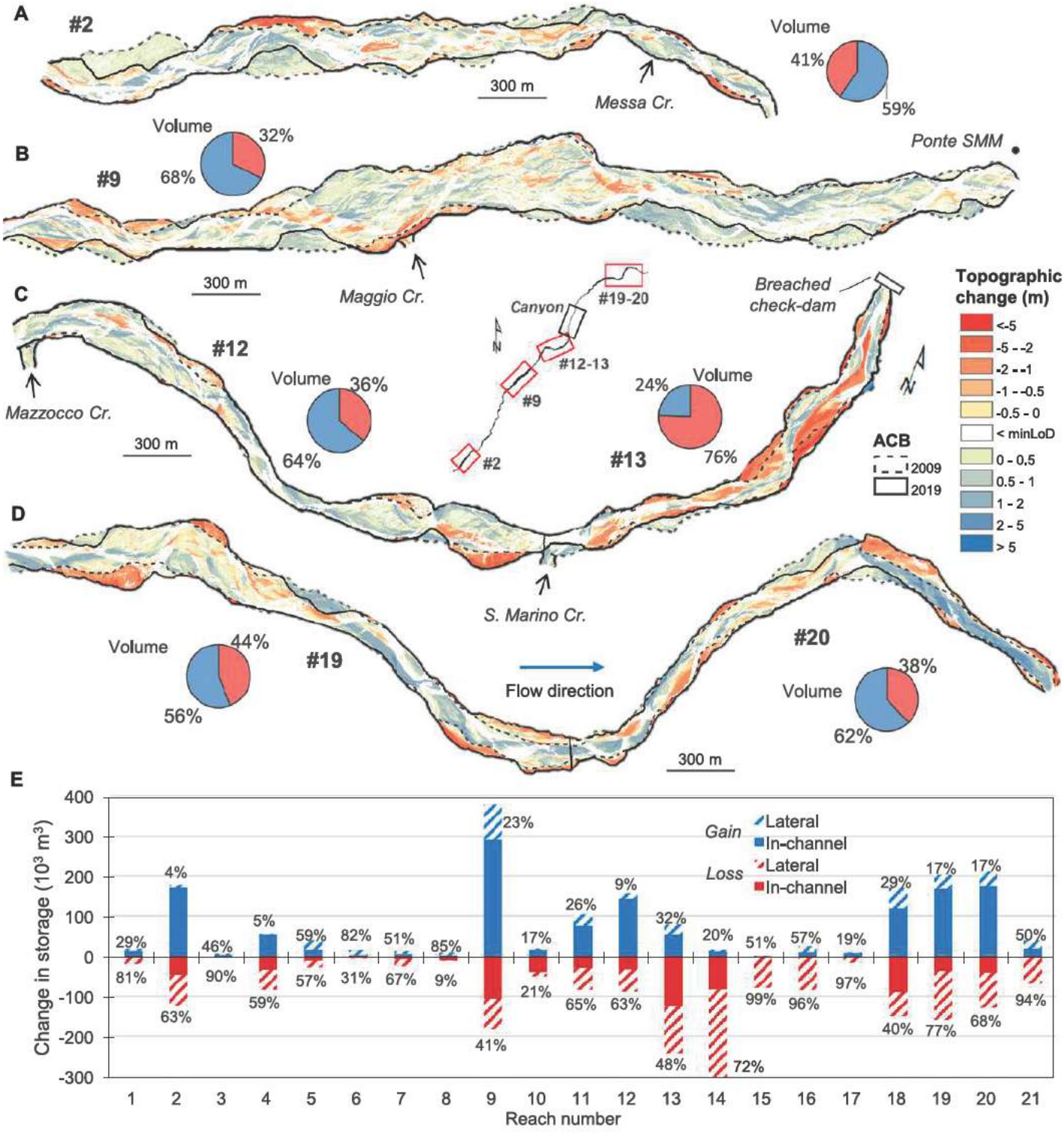

Figure 8. DEM (digital elevation model) of difference (DoD) maps within the combined footprint of the active channel bed (ACB) along reaches in 2009 (dashed linework) and 2019 (solid linework). (A) Reach 2, which corresponds to the Control 1 valley segment located downstream of the confluence with Senatello Creek; (B) reach 9, which corresponds to the Control 2 valley segment located upstream of Ponte S.M. Maddalena (SMM) gorge; (C) reaches 12 and 13, upstream of the canyon head at Ponte Verucchio; and (D) reaches 19 and 20, downstream of the canyon. (E) Stacked bar diagram illustrating the change in alluvial sediment storage across the 21 study reaches. Change in storage is subdivided into lateral and in-channel components (see Fig. 3A for definitions). Negative changes are referred to as degradation, and positive changes as aggradation. Pie charts indicate reach-based percentages of thresholded volume change associated with degradation (red sectors) and aggradation (blue sectors). Cr.—creek.

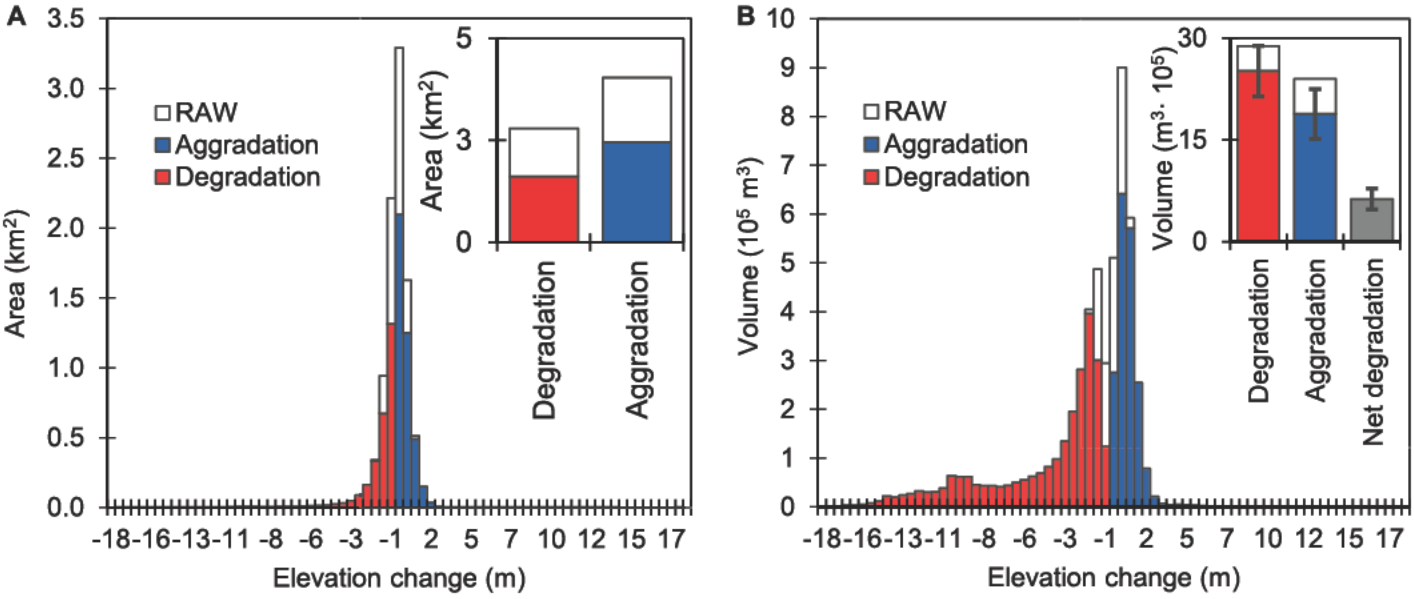

Figure 9. Size frequency distributions of the combined topographic changes observed along the entire Marecchia valley segment expressed by (A) area and (B) volume. Note that corresponding error values are +/–3.72 10^5 m^3 for degradation, +/–3.66 10^5 m^3 for aggradation, and +/–1.54 10^5 m^3 for net degradation. RAW—gross topographic changes.

to decline down to 80%–90%, with up to 8–10 m incision (e.g., Surian et al., 2009; Bollati et al., 2014; Scorpio et al., 2015). Even though working on unconfined reaches ensures experimental control, inevitably it provides only a partial view of the complexity characterizing mountain fluvial systems.

By considering the entire Marecchia River corridor, we document the variability of historical planimetric adjustment of a perturbed mountain fluvial system across channel segments that range in lateral confinement from 3% to 84%. Most importantly, with reference to the first objective of this paper, by exploiting spatially distributed detail of contemporary (i.e., 2009–2019) topographic change, we show how such systems respond to past anthropogenic disturbance through characteristic styles of (vertical and planimetric) adjustment in their building blocks i.e., the main alluvial reservoirs. In particular, we illustrate the extent to which an actively eroding canyon (section 5.3) can influence corridor-wide sediment dynamics (i.e., change in alluvial sediment storage) and more specifically, rates of sediment exchange with the modern alluvial floodplain.

Tracking historical change of active channel width across the main alluvial reservoirs provides preliminary hints about the likely functioning of the Marecchia River corridor since the onset of canyon incision (Fig. 4). Specifically, it suggests that propagation of the canyon sedimentary perturbation occurs in the downstream direction only, and that upstream of Ponte Verucchio, check dam planimetric trends of change mirror that of the headmost control reservoir (reach 2; Fig. 4). Specifically, narrowing between 1955 and 1996 follows a linear trend starting from "Control 1" down to "Control 2" and to the "Upstream" segment (Fig. 4). Further downstream, we observe a decoupled behavior, as the decline in active channel width is nonlinear along the canyon and in the "Downstream" segment. Decline is stronger (i.e., steeper) in the 1955–1969 period and weakens progressively through time. This dichotomic behavior between the upper and lower portions of the fluvial corridor continues after 1996, with planimetric change recorded at segment "Control 1" propagating down to "Control 2" (e.g., note maxima in ACW in 2006 and 2017, and minimum in 2012) and, although in an attenuated fashion, down to the "Upstream" segment, past Ponte S.M. Maddalena gorge (Fig. 4). Conversely, steady increase in active channel width in the canyon reflects down to the "Downstream" segment.

Integration of high-resolution volumetric channel changes that occurred between LiDAR acquisitions allows for an improved reading of transfer and storage dynamics across the array of sediment reservoirs, beyond gradation. In principle, the combination of lithological conditioning and historical anthropogenic forcing is expected to affect the characteristics of each reservoir, including channel slope and width, valley width, and therefore the degree of lateral confinement (Figs. 1, 2, and 6A). Confinement, in turn, by conditioning lateral sediment supply from hillsides and tributaries, as well as lateral migration potential, must have some bearing on the way in which each alluvial reservoir is capable to transport or store sediment through vertical and lateral adjustment (Lisle and Church, 2002).

The existence (and strength) of this structural conditioning was first suggested by the way steep, narrow, and confined reaches cluster away from gentler, wide, and weakly confined reservoirs (Fig. 7). Indeed, on one end of the spectrum we find a likely supply-limited cluster of reaches characterized by narrow, steep, and highly confined boundary conditions, including reach 3 (Ponte Messa), reach 10 (Ponte S.M. Maddalena), and the canyon (Fig. 7); on the opposite end sit the main alluvial reservoirs, bearing conditions compatible with a transport-limited regime (Dietrich et al., 1989; Montgomery and Buffington, 1997; Green et al., 2013).

Examination of change in alluvial storage (i.e., net change) further supports this view that style of adjustment, in reaches compatible with supply-limited conditions, would differ from transport-limited counterparts. In particular, we find the former reservoir type to be associated with negative and strongly negative changes in storage, whereas large, weakly unconfined reservoirs tend to accumulate additional sediment (Figs. 13A–13C). In the middle lie a number of partly confined reaches located between valley segments Control 1 and Control 2 (i.e., reaches 3 through 8) that display more balanced decadal budgets, hence suggesting they may act as graded transfer links (Fig. 13) as previously

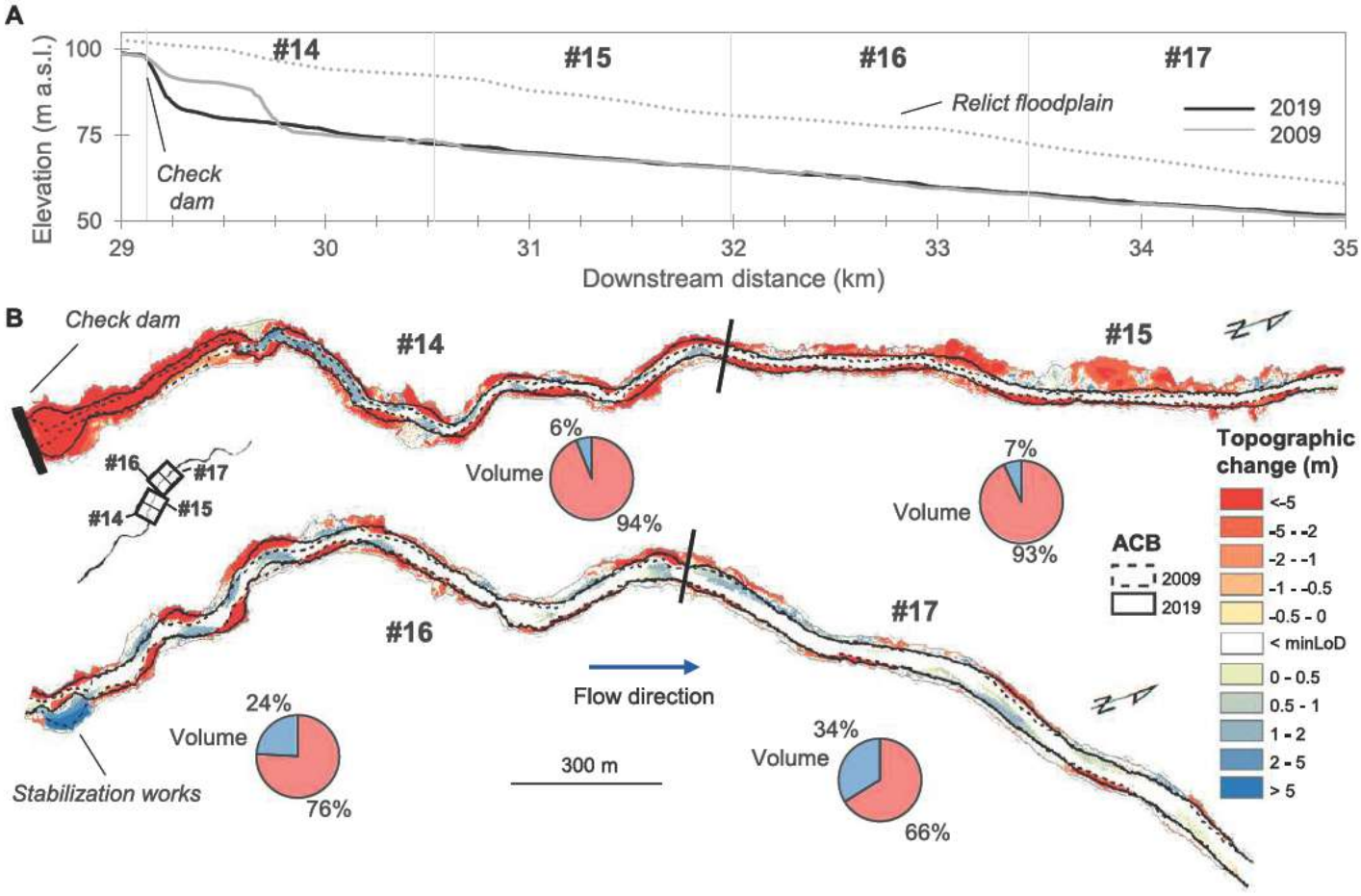

Figure 10. (A) Evolution of the canyon longitudinal profile between 2009 and 2019 showing knickpoint headward migration of ~500 m and concurrent vertical incision of ~10 m in the proximal portion of reach 14. Dotted linework indicates the level of the relict floodplain formerly occupied by the Marecchia River in 1955. (B) Maps of the DEM (digital elevation model) of difference (DoD) analysis conducted on a mask including the canyon walls, the footprints of landslides mapped in 2009 and 2019, and the extent of the Marecchia active channel bed (ACB) as mapped in 2009 (dashed linework) and 2019 (solid linework). Pie charts indicate reach-based percentages of thresholded volume change associated with degradation (red sectors) and aggradation (blue sectors).

implied by the nearly identical post-1996 trends in active channel width observed in the two control segments (Fig. 4).

Combined examination of lateral (widening or narrowing) and vertical (aggradation or degradation) channel changes allows: (1) gaining additional insights on the functioning of the alluvial reservoirs along the Marecchia corridor, including local transient effects associated with the collapse/deterioration of engineering structures; and (2) improving geomorphic inference, otherwise chiefly based on changes in active channel width. Although the study reaches encompass all four possible combinations of change, dominant styles of adjustment include degradation and widening ($n = 7$), as well as aggradation and narrowing ($n = 7$), with two reaches that have aggraded while widening, and two others that have degraded while becoming narrower (Fig. 13). When interpreting different adjustment styles, we should consider that these integrate changes occurred over a 10-yr snapshot, and therefore may not necessarily reflect simultaneous lateral and vertical channel changes, but sequences of in-channel and lateral variations that compete along a reach within this time window. In the following paragraphs, we encompass the different styles of reservoir adjustment and discuss their spatial distribution.

Widening and degradation dynamics characterize reaches responding either to long-term historical disturbance (i.e., gravel mining) or to more recent perturbations. The former include the four actively incising reaches of the canyon, which become progressively wider through hillslope-channel coupling (e.g., Figs. 5, 10, and 12); the latter include those that experienced major degradation following check dam failure during or shortly before the study period (i.e., reaches 10 and 13; Fig. 13). In particular, we propose that check dam failure in reach 13 may have triggered a complex pattern of adjustment across the entire reservoir, chiefly operated by widespread lateral migration that was fostered in part by increased slope gradient and flow divergence around mid-channel bars (note blue in-channel bands in Fig. 8C). In this context, we explain the behavior of reach 21 as the result of high artificial confinement (i.e., embankments for flood and avulsion prevention built at the entrance of Rimini) that has deteriorated locally, leading to bank erosion and channel widening (Fig. S5; see footnote 1).

Narrowing and concurrent gain in sediment storage characterize the major alluvial reservoirs in the upper and mid portions of the fluvial corridor (i.e., reaches 2, 9, 11, and 12). This style of adjustment exemplifies how, sometimes, making geomorphic inference based on changes in active channel width (i.e., considered as a

Figure 11. (A) Example of alluvium thickness (i.e., < 1 m) over sub-vertical pelitic layers (reach 15). Note the incipient slope undercutting at the base. (B) Talus deposit associated with a recent wall collapse (reach 16). (C) Toe of a rotational slide (left) moving to the right and deflecting water flow to the opposite canyon side, which consequently promotes undercutting (reach 15). (D) Point bars in a meandering stretch of the canyon (reach 16). Note the recent instability on the front wall induced by flow deflection at point bar.

proxy of bedload transport) may be misleading. Conceptually, reduction in active channel width in unconfined multi-thread reaches would be interpreted as diagnostic of reservoir depletion, channel incision, and/or reduced bedload transport; contrary to what is indicated by DoD maps and the relevant change in alluvial storage; i.e., note coexistence of high-magnitude aggradation and degradation volumes in reaches 2, 9, and 12 (Figs. 6C and 8). In this respect, the case of bed aggradation and narrowing in reaches 2 and 9 is useful. This apparently counter-intuitive style of adjustment derives from the initial emplacement of large lateral bars, which then stabilize and revegetate. In so doing, they become excluded from the active channel bed, which consequently narrows, getting incorporated (at least temporarily) into the alluvial floodplain (Figs. 8A and 8B). Similarly, partly confined reaches 3 through 8, while all narrowing, did not display univocal change in storage, but either a minor gain (i.e., reaches 5 and 6) or minor loss (i.e., reaches 4 and 7). Their minimal departures from balance further support our view that they may be regarded as graded, sedimentary transfer links.

Finally, widening and aggradation dynamics, which are found in reaches 19 and 20, reinforce previous planimetric-based interpretation of the evolution of the "downstream" valley segment (Fig. 4). This style of adjustment is compatible with that of depositional environments, where sediment supply exceeds transport capacity, as previously documented in unconfined lowland rivers (e.g., Ziliani and Surian, 2012; Bollati et al., 2014).

Considering the pelitic nature of its landslide-dominated walls, the canyon may be virtually regarded as a conveyor belt of bedload exiting reach 13 and a formidable source of suspended load. In particular, based on field estimations of thickness of the clastic alluvium stored over bedrock along the top margins of the canyon walls (i.e., the relict floodplain), we set the canyon bedload supply to the Marecchia River, via landsliding on the walls, to a conservative 10% of the total loss estimated through DoD analysis (e.g., thickness of alluvium over bedrock, where present, is typically less than 1 m on a 10-m-tall canyon wall; Fig. 11A). Following this logic, we interpret the highest rates of lateral channel instability in reaches 19 and 20 as a result of: (1) dramatic loss of stream power at the exit of the canyon (Fig. 6A), which favors widespread deposition of clastic sediment; and (2) high fine sediment supply from the canyon to substantially unconfined, transport-limited reaches (e.g., Venditti et al., 2010). In turn, widespread deposition of mid-channel bars (e.g., blue in-channel patches in Fig. 8D) induces flow divergence, leading to bar-lateral migration and intense bank erosion, and hence to channel widening. In this context, the balanced budget in reach 18 may exemplify graded river conditions, in which transport capacity equals sediment supply (Mackin, 1948). That is, at constant boundary conditions (i.e., constant water and sediment discharge), the stream would adjust to a constant transport capacity by altering other intrinsic channel characteristics in a complicated way (e.g., Cook et al., 2020). Following this logic, at the transition between confined (canyon) and unconfined (braided) conditions in reach 18, changes in slope and width, and potentially in roughness, may warrant constant transport capacity, and hence no change in storage.

The cumulative change in storage into lateral and in-channel components—where within the canyon the lateral component is not an actual change in alluvial storage, but represents landslide erosion of pelitic bedrock (Figs. 3B, 8E, and 11)—is instructive, as they display diverging downstream patterns (Fig. 14). In-channel change grows progressively downstream, thanks to the contribution of the largest natural reservoirs, tallying a cumulative gain of 333,000 m^3 at reach 9 and peaking at ~468,000 m^3 at reach 12. This pattern undergoes limited local depletion at reaches involved with structural failure (i.e., reaches 10 and 13) and along the canyon, where there is no substantial change downstream of its headmost reach (cf. Fig. 8D). Further down, strong increases in storage occur at reservoirs 19

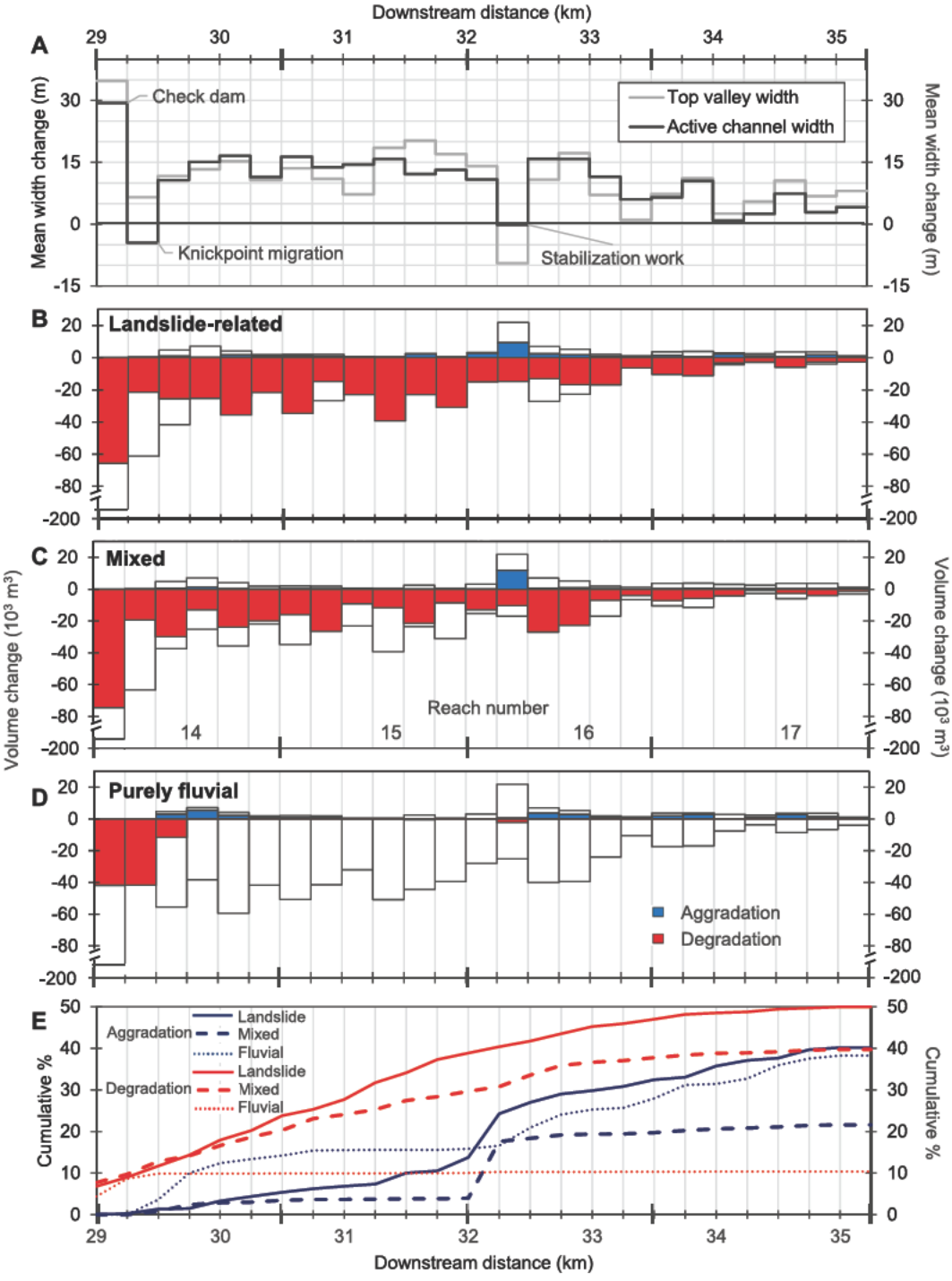

Figure 12. (A) Changes in top valley width and active channel width recorded in the Marecchia canyon between 2009 and 2019. Aggradation and degradation volumes are subdivided into (B) landslide-related, (C) mixed, and (D) purely fluvial components. Cumulative volumetric changes are illustrated in panel E.

and 20, where a cumulative gain of 651,000 m^3 is recorded.

As a consequence of prevalent degradation dynamics in 15 out of the 21 reaches (Fig. 8E), the cumulative downstream function of lateral change in storage differs markedly from the in-channel counterpart (Fig. 14). Its consistently negative pattern indicates the significance of sediment supplied to the active channel bed from the bordering floodplain through bank erosion, which is not countered by concurrent bar aggradation (e.g., Dunne et al., 1998). Main losses in the upper-to-mid portion of the corridor occur at reaches 2 and 4, and in reaches 11–13 (i.e., cumulative loss at reach 13 equals −256,000 m^3), so that by the end of the latter reach, the combined net budget is still positive for ~140,000 m^3 (i.e., black solid line in Fig. 14). Further downstream, ongoing canyon development in reaches 14–17 involves net lateral loss for over $1.1 \cdot 10^6$ m^3 (+/−0.3 10^6 m^3; thin dotted line in Fig. 14), leading to a dramatic combined deficit.

However, since this loss is chiefly associated with pelitic bedrock erosion (i.e., 90% of the DoD-based degradation; e.g., Fig. 11A), most of the sediment supply goes into suspension and travels to the Adriatic Sea, likely providing a nearly negligible contribution to detectable thresholded DoD changes in comparison to a

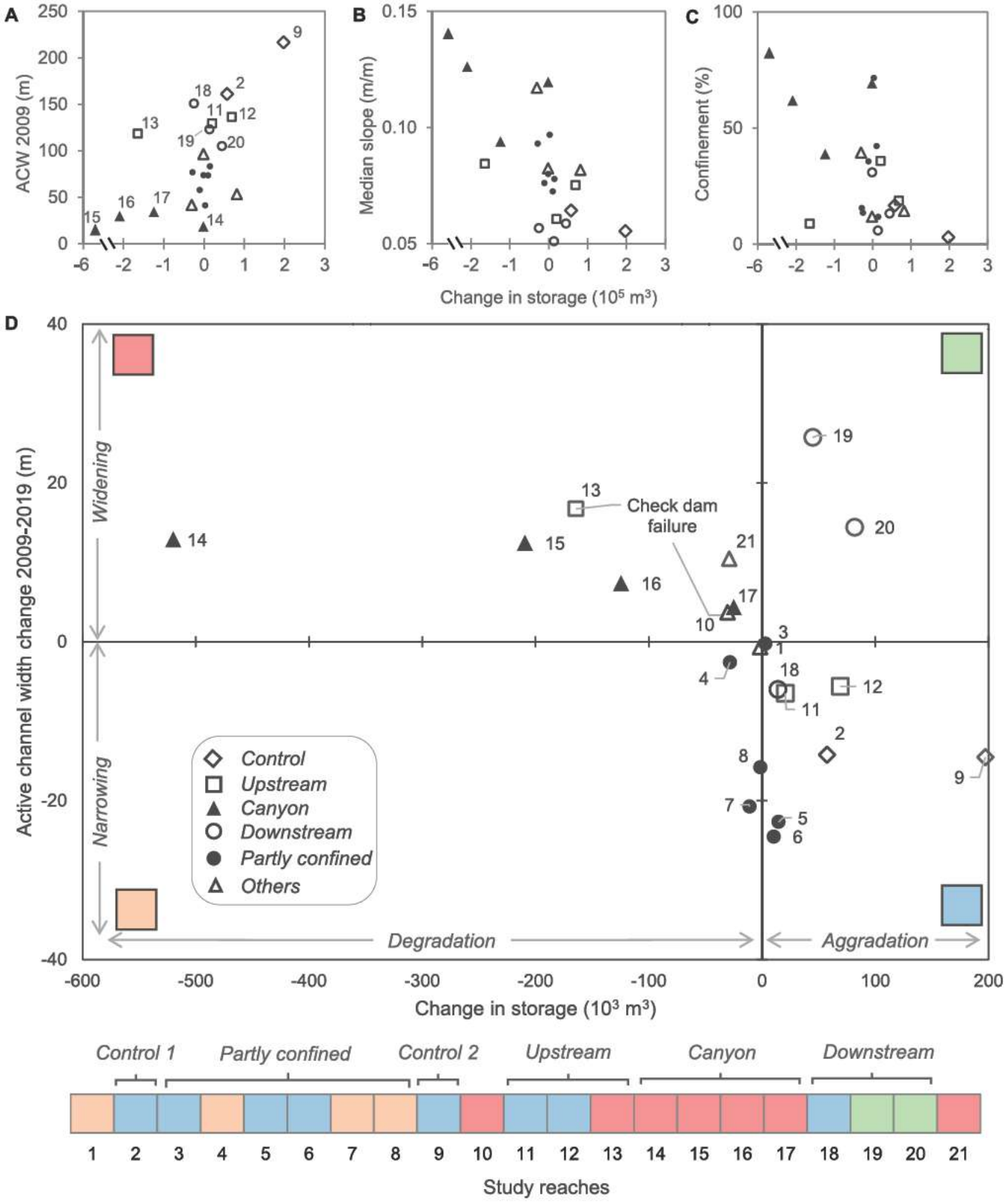

Figure 13. Reach-based scatterplots showing change in storage as a function of (A) active channel width (ACW), (B) median slope, (C) confinement, and (D) change in ACW. In panel D, to provide a general overview of the spatial organization of the sediment reservoirs along the Marecchia River corridor, reaches are represented as arrays of squares with different shades depending on the combined style of lateral and vertical adjustment.

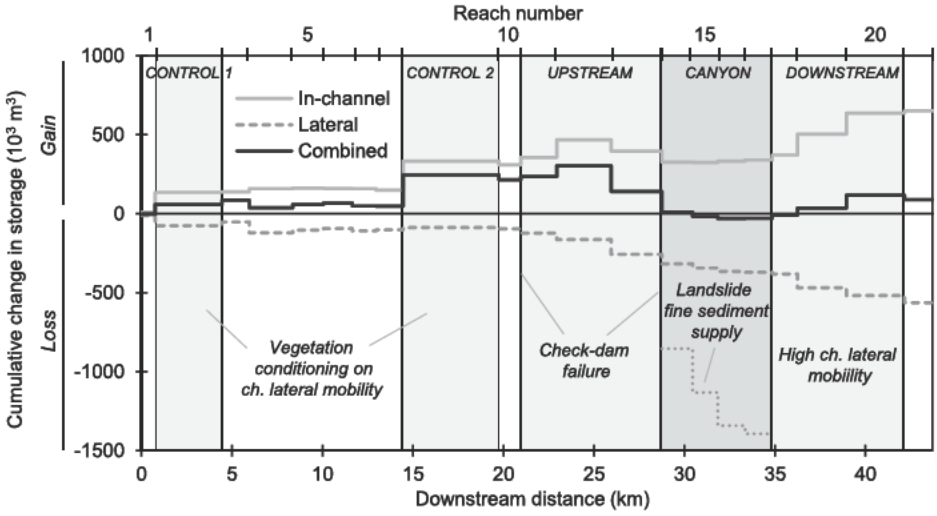

Figure 14. Cumulative change in alluvial storage along the Marecchia River corridor (combined) and relevant decomposition into in-channel and lateral components (Fig. 3A). Within the canyon (reaches 14–17), the lateral component includes loss of storage (i.e., 10% of the degradation calculated via thresholded DoD analysis) operated by landsliding (i.e., landslide-related component) and hillslope-channel coupling (i.e., mixed component; Figs. 3B and 12). Dotted linework within the canyon indicates the total loss of volume associated with the erosion of the pelitic bedrock (90%) and the stripping of the alluvium (10%) from the relict floodplain.

supply that entered the bedload fraction (e.g., Whiting et al., 2005; Kasprak et al., 2015; Franz et al., 2017). This assumption is confirmed by the very limited amount of channel aggradation observed along the distal reaches of the canyon (Figs. 10 and 12D). Following this logic, we set cumulative change in storage to resume past the canyon at the same deficit level recorded at reach 13 (−256,000 m³ +/−38,400 m³) and augmented it by the loss in bedload material stripped from the relict floodplain through landsliding—i.e., 10% of DoD volumetric degradation associated with the landslide-related and the mixed components (–382,000 m³). Downstream of the canyon, lateral loss in storage continues to grow across reaches 19–21, attaining a value of about −563,000 m³ (+/−135,000 m³), which leads, at the end of the study corridor, to a combined gain of 88,000 m³ (+/−21,000 m³).

Based on the foregoing spatial variability in cumulative change in storage, the fluvial corridor may be subdivided into three main zones, each of which possibly requires specific management strategies. These include: (1) an upper zone characterized by a substantial gain in alluvial storage and modest lateral migration chiefly controlled by riparian vegetation dynamics; (2) the inherited, actively eroding canyon that forms a major source of suspended load and virtually acts as a bedload conveyor belt; and (3) the distal depositional zone characterized by high lateral mobility, and hence by the highest rates of sediment exchange between the active channel and the modern floodplain.

Large sediment supply associated with bank erosion has been documented elsewhere in riverine environments (e.g., Church et al., 1989; Dunne et al., 1998; Simon et al., 2000; Simon and Rinaldi, 2006; Parker et al., 2008). Sediment exchange rates between the main channel and the floodplain were found to exceed rates of downstream transport in the Amazon, where contrary to the Marecchia River, dynamics of lateral bar deposition overcome losses associated with bank erosion (Dunne et al., 1998). Rinaldi and Darby (2008), in unstable and incised streams in the UK, as well as Simon et al. (1996) across streams of the midcontinent of the United States, report bank erosion as the main source of sediment, contributing up to 80% of the total sediment yield. Church and Slaymaker (1989), in formerly glaciated British Columbia, linked the regional pattern of modern clastic sediment yield to the ongoing massive reworking of sediment stored in glacial and postglacial deposits, recruited through bank erosion.

Quantitative information about tributary sediment fluxes entering the Marecchia River is limited to the largest one, the Mazzocco (47 km²), which directly feeds reach 12 (Figs. 8C and 14). DoD (2009–2019) analysis along its 10-km course indicates that this tributary contribution may be episodically important, as evidenced by a net storage loss of ∼14,000 m³ (+/−2520 m³) (Fig. S6), which accounts for 60% of the net gain observed in reach 12 across the same period. By contrast, the contribution of San Marino Creek (37 km²), the second largest tributary entering the Marecchia River in reach 13, appears to be much lower in comparison (cf. Figs. S7 and S8; note the lack of sediment storage sites in San Marino), as no substantial planform changes are observed between 2006 and 2019.

5.2. Transient Evolution of the Marecchia River Canyon

Channel incision and concurrent lateral migration typically make the adjacent banks (or hillslopes) more vulnerable by increasing their slope gradients and heights (i.e., local relief), up to a point where gravitational forces during a flood event will exceed shear strength, resulting in mass failure (Osman and Thorne, 1988; ASCE Task Committee on Hydraulics, Bank Mechanics and Modeling of River Width Adjustment, 1998; Langendoen and Simon, 2008). In the same way, knickpoint headward migration through a bedrock channel induces local incision, which in turn evolves into a perturbation on the adjacent slopes. This perturbation can be almost instantaneous, triggering short-term feedback mechanisms of adjustment (Golly et al., 2017), or last up to post-orogenic times (Gallen et al., 2011). Thus, at a fundamental landscape evolution level, river canyons carved into bedrock develop via a feedback mechanism that links deepening and widening through fluvial incision. In turn, widening, depending on the fabric of the confining walls, may be further promoted by hillslopes responding to fluvial incision through landsliding and, in soil-mantled landscapes, via other diffusive processes, such as soil creep and frost heave (e.g., Mudd and Furbish, 2007; Attal et al., 2015). In this context, through a 10-yr natural experiment, we constrained rates of valley incision and widening into weak pelitic bedrock (Fig. 12), while identifying changing styles of hillslope-channel coupling down the canyon (Figs. 10B, 11, and 15). In particular, this lithological setting offers an opportunity to examine canyon development with reasonable experimental control, that is, away from possible negative feedbacks induced by coarse-grained hillslope sediment supply (e.g., Johnson and Finnegan, 2015; Shobe et al., 2016; Glade et al., 2019).

With reference to the second objective of this paper, our analysis depicts a striking case of transient geomorphic response to anthropogenic disturbance, triggered between the late 1940s and the early 1950s by widespread gravel mining activity in the Marecchia River's distal reaches. In the 10-yr snapshot under investigation, tran-

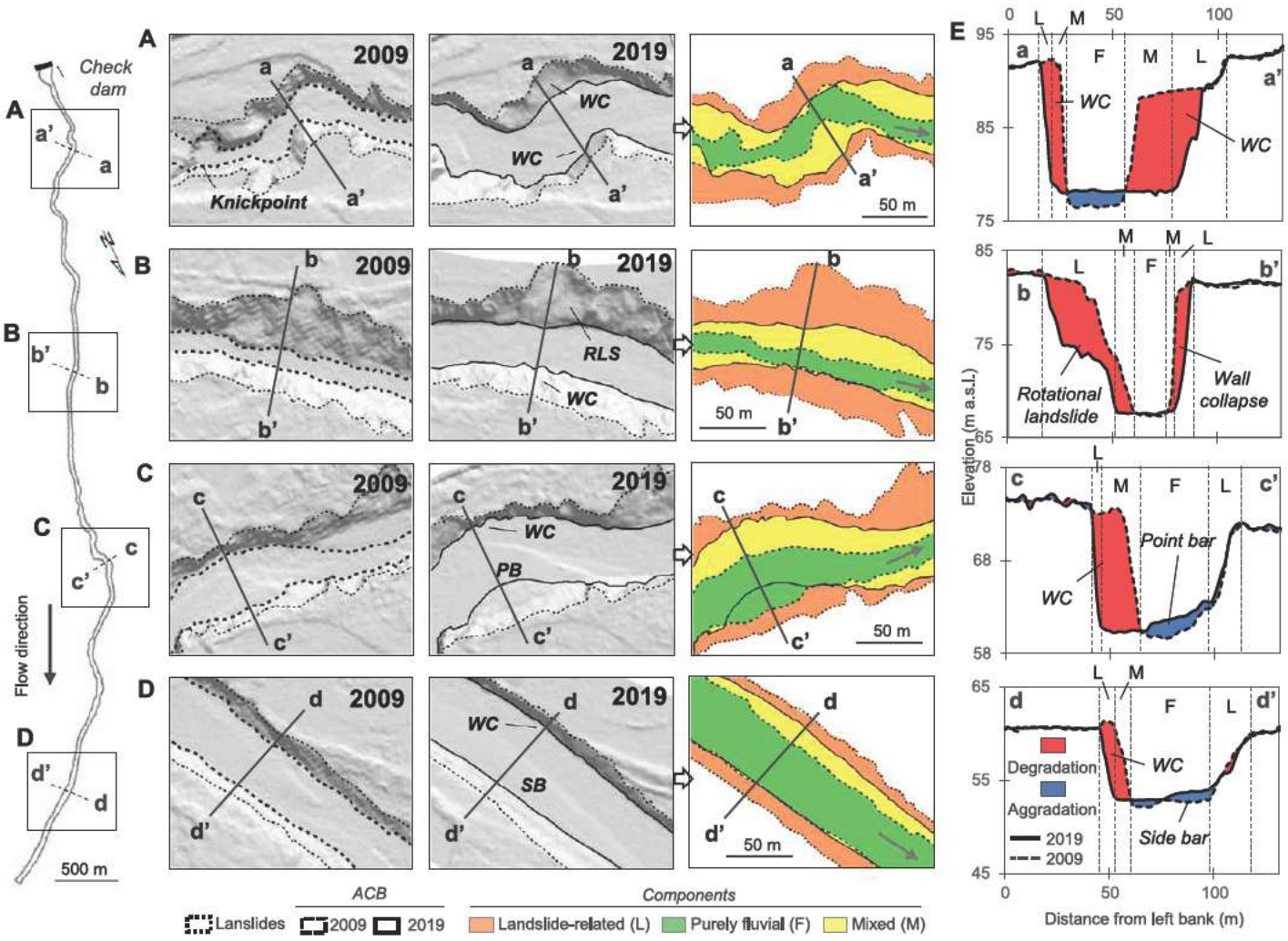

Figure 15. Plan views and cross sections of sample valley stretches within the canyon showing changes between 2009 and 2019 as result of different styles of hillslope-channel coupling. Note the reduction in wall height from proximal to distal cross sections. For definitions of landslide-related, purely fluvial, and mixed components, refer to Figure 3B. For corresponding orthophotos of the sample canyon stretches, refer to Figure S9 (see text footnote 1). WC—wall collapse; PB—point bar; RLS—rotational landslide; SB—side bar.

science manifests through high geomorphic activity at the canyon head, which weakens progressively, moving down to the "older" distal portions (Figs. 10 and 12). In particular, high headmost activity consists of waterfall erosion (e.g., Lamb et al., 2007; Lapotre et al., 2016; Scheingross and Lamb, 2017), which has led to knickpoint migration of ~500 m (i.e., 50,000 mm/yr on average) and to an average incision depth of 9 m (i.e., 900 mm/yr on average; Fig. 10). These decadal rates of bedrock wearing are well above the averages documented by prior work on canyon evolution in natural settings, both in terms of knickpoint migration, which typically ranges between <10 mm/yr (e.g., Bishop et al., 2005; Whittaker and Boulton, 2012) and up to ~1000 mm/yr (e.g., Hayakawa and Matsukura, 2003; Baynes et al., 2015); and in terms of channel bed incision, which have been documented to vary between <1 mm/yr (e.g., Reusser et al., 2004; Cyr and Granger, 2008; Sanders et al., 2014) over millennial temporal scales, and ~100 mm/yr (e.g., James, 2004; Stock et al., 2005) over decades. Comparable or higher rates of change through days, or a few years, have only been observed following catastrophic events, such as megafloods or earthquakes (e.g., Lamb and Fonstad, 2010; Cook et al., 2013). For example, in a 4-yr monitoring period, following co-seismic bedrock uplift, in Da'an River, Taiwan, Cook et al. (2013) report average incision of 5 m/yr in weakly consolidated sedimentary rock, for a resulting knickpoint migration rate of 155 m/yr. Over 6 years, Anton et al. (2015) reported an average incision rate of 17 m/yr and knickpoint migration of 45 m/yr in a granitic bedrock reach of Esla River, Spain, following the overtopping of a rock-cut dam spillway during small-to-moderate floods.

Downstream of the headmost 750 m, vertical incision drops abruptly to nearly negligible rates (Fig. 12D). By contrast, valley widening, chiefly operated by landslide activity in tandem with fluvial undercutting—expressed here as volume loss of the landslide-related (Fig. 12B) and mixed components (Fig. 12C)—displays a transient downstream pattern on both walls and declines nonlinearly across the entire canyon length (Figs. 12B, 12C, and 12E). Accordingly, rates of top valley widening are highest at the canyon head (3.5 m/yr on average), set to ~1.5 m/yr in its upper half, and decline to an average of 0.7 m/yr further downstream (Fig. 12A). These volumetric and geometric

rates of change are associated with varying styles of failure, which encompass some of the bank retreat mechanisms characterizing incised alluvial streams (e.g., ASCE Task Committee on Hydraulics, Bank Mechanics and Modeling of River Width Adjustment, 1998; Langendoen and Simon, 2008). Accordingly, in the upper half of the canyon, where both side walls are actively degrading, the orientation of the pelitic layers dictates failure type, in that low-angle rotational slides occur on the valley side with pelitic layers dipping toward the channel bed. In turn, slide toes deflect water flow toward the opposite valley side (e.g., Fig. 11C), inducing slope undercutting and ultimately leading to canyon-wall collapses and toppling (e.g., Fig. 11B). Even though, from a plan view perspective, vertical collapses may appear secondary to rotational and planar slides, the high volume–area ratio makes them prominent mechanisms both in terms of canyon widening and sediment supply (e.g., Langendoen and Alonso, 2008). Further downstream, where canyon wall failures become smaller and less pervasive, erosional patches alternate to depositional point bars in sinuous stretches (Figs. 10 and 15C), and to side bars in more rectilinear ones (Figs. 10 and 15C).

Unexpectedly, canyon depth appears to increase upstream, when moving from old to younger reaches (Fig. 15D), suggesting that the canyon head, while migrating upstream, has evolved to a progressively more unstable configuration—shear stress at the base of a sub-vertical earth wall increases directly with wall height, hence making taller pelitic walls more prone to fail (e.g., Janbu et al., 1956)—which likely has fostered more efficient incision into bedrock through time. This observation points to canyon development that—following alluvium removal, substrate exposure, and local base-level fall caused by gravel mining—nowadays proceeds through knickpoint retreat, a style of adjustment that in stream-power numerical simulations, and subsequent empirical work, has been associated with detachment-limited conditions, as opposed to a diffusive style indicative of transport limitation (Whipple and Tucker, 2002; Jansen et al., 2011). Most importantly, it reinforces prior empirical work and interpretations—rooted in the saltation-abrasion model (Sklar and Dietrich, 2004)—of a possible runaway style of evolution, according to which, a perturbation of a given magnitude can lead to greater rates of change through bedrock incision (e.g., Cook et al., 2013; Finnegan and Balco, 2013). Following this logic, in the Marecchia River canyon, the incision of a progressively deeper head would be driven by bedload wearing on highly erodible bedrock walls. To test whether the carving of an increasingly deeper gorge in more recent decades was paralleled by higher erosion rates—a question that holds critical implications for the formation and interpretation of strath terraces—future work in the Marecchia River will aim to reconstruct both canyon geometry and volumetric rates of bedrock incision since the onset of canyon development in the 1950s.

5.3. Uncertainties

A number of uncertainties affect our evaluations of planimetric and vertical channel adjustments. In this section, we focus on some fundamental issues related to the estimation of the active channel width, the evaluation of decadal topographic changes that occurred between the sequential airborne LiDAR acquisitions, and the limitations associated with the temporal resolution of the historical (1955–2019) and decadal (2009–2019) analyses.

In historical aerial photos ranging in nominal scale between 1:7000 and 1:55,000, maximum planimetric offset associated with the manual mapping of the active channel bed and the calculation of the active channel width—which relates both to alignment/distortion among the sequential orthophoto mosaics and to the mapper's experience—has been found to vary between 5 m and 6 m (e.g., Gurnell, 1997; Hughes et al., 2006; Surian et al., 2009). These figures apply to the coarsest orthophoto mosaic (pixel size = 1 m) derived from aerial photos taken in 1955 (nominal scale 1:55,000) and decline to a maximum of 2 m for post-1985 photo years, where the nominal scale ranges from 1:7000 to 1:13,000, and pixel size from 0.2 m (e.g., 2019) to 0.5 m (e.g., 2009). In the 2009–2019 period, uncertainty about active channel delineation was further reduced through visual inspection of LiDAR-derived shaded relief imagery. To reduce the degree of subjectivity, the original manual mapping was revised by two additional operators until a consensus was reached. The cumulative effects of the foregoing uncertainties, especially when averaged at the valley segment (Fig. 4) and the reach scales (Figs. 6A, 6B, and 7), lead to minor shifts on the relevant diagrams and scatterplots that we believe would not significantly modify historical and decadal trends in active channel width (Figs. 4 and 6). Similarly, we believe that the sign and strength of the correlations of active channel width with median reach slope and confinement would not change appreciably (Fig. 7).

Evaluation of volumetric channel changes is affected by both the quality of the LiDAR-derived DEMs, as well as by the temporal resolution associated with the DoD analysis. Errors in topographic surveys propagate into uncertainties in the estimates of volumetric channel changes (e.g., Brasington et al., 2000; Wheaton et al., 2010), and therefore may affect the partitioning of volumetric changes into aggradation, degradation, and resulting net change. These uncertainties may be particularly relevant in environments, or over temporal scales, in which vertical topographic changes are relatively low compared to the errors associated with the sequential DEMs. To disentangle real topographic changes from noise, we applied a rather conservative thresholding to the DoD analysis (i.e., 95% confidence level; see section 3).

To test the extent to which our approach to uncertainty regarding the sequential DEM surfaces may affect one of the key channel variates examined in this work, we compared the cumulative thresholded change in storage with the "raw" (non-thresholded) counterpart (Fig. S10; see footnote 1). Results show that thresholded estimates of cumulative change in storage are consistently greater, except for slight underestimations in reaches 14–18. Most importantly, the shapes of the two cumulative functions down the Marecchia River corridor mirror each other (Fig. S10C), with a consistent sign of variation (i.e., gain or loss of storage) across all of the study reaches (cf. net change in Table S2, and Figs. S11A and S11B), indicating that our evaluation of volumetric changes is robust despite the associated uncertainties.

The temporal resolution of the analysis of topographic channel changes between 2009 and 2019 is determined by the available LiDAR surveys, and this time period integrates the geomorphic effects of multiple floods (i.e., five >2-yr peak flows; Fig. 2D). The evaluation of alluvial sediment budgets is known to be negatively biased by local scour-and-fill compensations that occur between surveys, which typically remain undetected (e.g., Lindsay and Ashmore, 2002). Although this may represent a critical limitation in studies concerned with the monitoring of sediment transport and river morphodynamics at the flood-event scale, it does not invalidate our work, considering the focus on change in alluvial storage at the decadal scale and that no extreme flood event has occurred within the study period. In this context, visual inspection of photo years 2012, 2014, and 2017 proved useful for consolidating interpretations of the 2009–2019 DoD maps (for example, the effects of check dam failures).

6. CONCLUSIONS

By integrating the historical (i.e., 1955–2019) planimetric evolution of the active channel bed with the contemporary (i.e., 2009–2019) LiDAR-derived topographic change, we infer decadal sediment dynamics along the array of

diverse sediment reservoirs in the perturbed Marecchia River corridor.

Reconstruction of post-1955 channel-planform changes, complemented by historical cross-sectional surveys, depict a split river system with distinctive trends of variation observed in valley segments located, respectively, downstream and upstream of the canyon, which forms an element of discontinuity and appears to condition the variation of active channel width in the downstream direction. Conversely, we show that in the upper portion of the river, the historical trend of planform-channel change, as recorded at the headmost main alluvial reservoir (i.e., reach 2), propagates virtually unchanged to the next one (i.e., reach 9) through a series of narrower and partly confined reaches, and further downstream past a bedrock gorge, even though substantially attenuated. In particular, since the mid-1990s—after 40 years of continuous narrowing—active channel width in the main alluvial reservoirs upstream of the canyon appears to have attained a new stage of dynamic equilibrium, whereas incremental adjustment (i.e., progressive widening) persists downstream.

In this historical context, geomorphic change detection performed on sequential LiDAR-derived DEMs allows improved understanding of how single reservoirs (i.e., channel reaches) tend to adjust, depending on their positioning within the inherited, perturbed fluvial landscape and on local perturbations. In particular, we find that decadal change in sediment storage across reaches correlates with supply- and transport-limited boundary conditions, as constrained by the degree of lateral confinement, stream channel slope, and active channel width. Accordingly, steep, narrow, and tightly confined reaches are associated with negative and strongly negative changes in storage; large, weakly confined reservoirs tend to accumulate additional storage; and partly confined counterparts display more balanced budgets, substantially behaving as graded transfer links.

In turn, this first-order classification scheme helps to explain the different styles of lateral and vertical channel-reach adjustment, which are more composite than as inferred solely based on variations in active channel width. For example, we show that over a decade, planimetric widening can occur along strongly degrading reaches—in response either to long-term disturbance (i.e., historical gravel mining) along the canyon, or to recent short-lived perturbations following check dam failure—as well as in strongly aggrading counterparts, as exemplified by the unconfined, multi-thread distal reservoirs located downstream of the canyon (i.e., reaches 19 and 20). Likewise, substantial gain in alluvial storage may also occur in reservoirs experiencing contingent narrowing—due to lateral bar revegetation and subsequent temporary incorporation into the adjacent floodplain stock—such as in the upper half of the corridor (i.e., reaches 2, 9, 11, and 12). Collectively, different styles of decadal (lateral and vertical) adjustment point to contrasting stages of evolution at reservoirs located downstream and upstream of the canyon head, thus corroborating the split geomorphic behavior (i.e., transient response versus dynamic equilibrium) previously hypothesized through interpretation of historical planimetric channel changes.

Decomposition of change in storage into in-channel and lateral components further contributes to elucidating the causes of the spatial variability observed in the corridor's budget. In particular, we find that the relevant cumulative functions depart markedly from one another. The in-channel component grows progressively downstream across the main wide, unconfined, and multi-thread natural reservoirs (i.e., reaches 2, 9, 12, 19, and 20), with depletions focused on sites experiencing check dam failure and at the canyon head. The lateral component displays dominant degradation dynamics, with loss in storage growing consistently downstream of Ponte S.M. Maddalena gorge (i.e., reach 10). The highest losses are recorded downstream of the canyon (i.e., reaches 19 and 20), where high inputs of fine sediment imparts widespread lateral channel instability. This spatial pattern of lateral degradation highlights the geomorphic significance of sediment supply from the bordering floodplain (through bank erosion) and the canyon walls (through landsliding) to the lower half of the Marecchia River bed, which is not balanced by concurrent aggradation at point and lateral bars. Indirectly, it also stresses the importance of leaving a riparian buffer for channel-lateral migration and bedload recruitment against sediment starvation.

From a landscape evolution standpoint, our 10-yr natural experiment allows constraining rates of canyon development into weak pelitic bedrock that are well above averages reported by prior work conducted in other natural settings. In particular, we document a clear case of transient geomorphic response to anthropogenic forcing, where transience, modulated by changing styles of hillslope-channel coupling, manifests through high geomorphic activity at the canyon head and then declines nonlinearly downstream. Most importantly, we find that canyon depth increases upstream, which suggests that the canyon head has been evolving toward a more unstable geometric configuration. This observation may mean that relevant rates of bedrock erosion have progressively grown larger since the canyon carving began, with basic implications for our understanding of channel incision into bedrock and strath terrace formation, as well as practical consequences for infrastructures located upstream. Beyond the Marecchia case study, by showing that mining alluvial gravel down to bedrock may constitute an efficient anthropogenic mechanism of strath formation—in addition to reduced sediment retention following splash-dam logging (Schanz et al., 2019)—we conclude that anthropogenic straths may be more widely distributed than previously envisaged (Schanz et al., 2018), and that straths may also form without a significant change in sediment supply.

ACKNOWLEDGMENTS

This work was jointly funded by the University of Bologna and the Autorità di Bacino Distrettuale del Fiume Po (AdBPo). We acknowledge collaborative support granted by personnel of Regione Emilia-Romagna (through ARPAE, Agenzia per la sicurezza territoriale e la protezione civile, and Servizio difesa del suolo, della costa e bonifica) for hydrological and cross-sectional data sharing. We thank Stefano Conti and Olivia Nesci for sharing knowledge about the geology and geomorphology of the Marecchia River basin. Stimulating discussions with Noah Finnegan on an earlier version of the manuscript helped highlight insights into incision and strath formation. The paper benefitted from two anonymous constructive reviews that greatly improved the structure and clarity of this work.

REFERENCES CITED

ARPAE (Agenzia per la sicurezza territoriale e la protezione civile, and Servizio difesa del suolo, della costa e bonifica), 2019, Annali Idrologici 2019: Parte Seconda: Struttura Idro-Meteo-Clima Servizio idrografia e idrologia regionale e distretto Po, 154 p.

ASCE Task Committee on Hydraulics, Bank Mechanics and Modeling of River Width Adjustment, 1998, River width adjustment. I: Processes and Mechanisms: Journal of Hydraulic Engineering, v. 124, no. 9, p. 881–902, https://doi.org/10.1061/(ASCE)0733-9429(1998)124:9(881).

Anton, L., Mather, A.E., Stokes, M., Muñoz-Martin, A., and De Vicente, G., 2015, Exceptional river gorge formation from unexceptional floods: Nature Communications, v. 6, 7963, https://doi.org/10.1038/ncomms8963.

Attal, M., Mudd, S M., Hurst, M.D., Weinman, B., Yoo, K., and Naylor, M., 2015, Impact of change in erosion rate and landscape steepness on hillslope and fluvial sediments grain size in the Feather River basin (Sierra Nevada, California): Earth Surface Dynamics, v. 3, p. 201–222, https://doi.org/10.5194/esurf-3-201-2015.

Baynes, E.R.C., Attal, M., Niedermann, S., Kirstein, L.A., Dugmore, A.J., and Naylor, M., 2015, Erosion during extreme flood events dominates Holocene canyon evolution in northeast Iceland: Proceedings of the National Academy of Sciences of the United States of America, v. 112, no. 8, p. 2355–2360, https://doi.org/10.1073/pnas.1415443112.

Benda, L., and Dunne, T., 1997, Stochastic forcing of sediment routing and storage in channel networks: Water Resources Research, v. 33, no. 12, p. 2865–2880, https://doi.org/10.1029/97WR02387.

Benda, L., Miller, D., Dunne, T., Agee, J., and Reeves, G., 1998, Dynamic landscape systems, *in* Naiman, R., and Bilby, R., eds., River Ecology and Management: Lessons from the Pacific Coastal Ecoregion: Springer-Verlag, p. 261–288, https://doi.org/10.1007/978-1-4612-1652-0_11.

Bertrand, M., and Liébault, F., 2019, Active channel width as a proxy of sediment supply from mining sites in New

Caledonia: Earth Surface Processes and Landforms, v. 44, p. 67–76, https://doi.org/10.1002/esp.4478.
Bishop, P., Hoey, T.B., Jansen, J.D., and Artza, I.L., 2005, Knickpoint recession rate and catchment area: The case of uplifted rivers in Eastern Scotland: Earth Surface Processes and Landforms, v. 30, p. 767–778, https://doi.org/10.1002/esp.1191.
Bollati, I.M., Pellegrini, L., Rinaldi, M., Duci, G., and Pelfini, M., 2014, Reach-scale morphological adjustments and stages of channel evolution: The case of the Trebbia River (northern Italy): Geomorphology, v. 221, p. 176–186, https://doi.org/10.1016/j.geomorph.2014.06.007.
Brardinoni, F., and Hassan, M.A., 2007, Glacially induced organization of channel-reach morphology in mountain streams: Journal of Geophysical Research: Earth Surface, v. 112, https://doi.org/10.1029/2006JF000741.
Brardinoni, F., Picotti, V., Maraio, S., Bruno, P.P., Cucato, M., Morelli, C., and Mair, V., 2018, Postglacial evolution of a formerly glaciated valley: Reconstructing sediment supply, fan building, and confluence effects at the millennial time scale: Geological Society of America Bulletin, v. 130, p. 1457–1473, https://doi.org/10.1130/B31924.1.
Brasington, J., Rumsby, B., and McVey, R., 2000, Monitoring and modelling morphological change in a braided gravel-bed river using high resolution GPS-based survey: Earth Surface Processes and Landforms, v. 25, p. 973–990, https://doi.org/10.1002/1096-9837(200008)25:9<973::AID-ESP111>3.0.CO;2-Y.
Brenna, A., Bizzi, S., and Surian, N., 2022, A width-based approach to estimating historical changes in coarse sediment fluxes at river reach and network scales: Earth Surface Processes and Landforms, v. 47, p. 2560–2579, https://doi.org/10.1002/esp.5395.
Brummer, C.J., and Montgomery, D.R., 2003, Downstream coarsening in headwater channels: Water Resources Research, v. 39, no. 10, https://doi.org/10.1029/2003WR001981.
Brunsden, D., and Thornes, J.B., 1979, Landscape sensitivity and change: Transactions of the Institute of British Geographers, v. 4, p. 463–484, https://doi.org/10.2307/622210.
Caine, N., and Swanson, F.J., 1989, Geomorphic coupling of hillslope and channel systems in two small mountain basins: Zeitschrift für Geomorphologie, v. 33, no. 2, p. 189–203, https://doi.org/10.1127/zfg/33/1989/189.
Cantelli, A., Paola, C., and Parker, G., 2004, Experiments on upstream-migrating erosional narrowing and widening of an incisional channel caused by dam removal: Water Resources Research, v. 40, https://doi.org/10.1029/2003WR002940.
Church, M., 2006, Bed material transport and the morphology of alluvial river channels: Annual Review of Earth and Planetary Sciences, v. 34, no. 1, p. 325–354, https://doi.org/10.1146/annurev.earth.33.092203.122721.
Church, M., and Slaymaker, O., 1989, Disequilibrium of Holocene sediment yield in glaciated British Columbia: Nature, v. 337, p. 452–454, https://doi.org/10.1038/337452a0.
Church, M., Kellerhals, R., and Day, T.J., 1989, Regional clastic sediment yield in B.C: Canadian Journal of Earth Sciences, v. 26, p. 31–45, https://doi.org/10.1139/e89-004.
Comiti, F., 2012, How natural are Alpine mountain rivers?: Evidence from the Italian Alps: Geomorphology, v. 37, p. 693–707.
Conti, P., Cornamusini, G., and Carmignani, L., 2019, Carta Geologica delle Regioni Emilia-Romagna, Marche, Toscana e Umbria (Note illustrative della Carta Geologica alla scala 1:250 000): Archivio cartografico della Regione Emilia-Romagna, scale 1:250,000, 80 p.
Conti, S., Fioroni, C., Fontana, D., and Grillezoni, C., 2016, Depositional history of the Epiligurian wedge-top basin in the Val Marecchia area (northern Apennines, Italy): A revision of the Burdigalian–Tortonian succession: Italian Journal of Geosciences, v. 135, no. 2, p. 324–335, https://doi.org/10.3301/IJG.2015.32.
Cook, K.L., Turowski, J.M., and Hovius, N., 2013, A demonstration of the importance of bedload transport for fluvial bedrock erosion and knickpoint propagation: Earth Surface Processes and Landforms, v. 38, p. 683–695, https://doi.org/10.1002/esp.3313.
Cook, K.L., Turowski, J.M., and Hovius, N., 2020, Width control on event-scale deposition and evacuation of sediment in bedrock-confined channels: Earth Surface Processes and Landforms, v. 45, no. 14, p. 3702–3713, https://doi.org/10.1002/esp.4993.
Cyr, A.J., and Granger, D.E., 2008, Dynamic equilibrium among erosion, river incision, and coastal uplift in the northern and central Apennines, Italy: Geology, v. 36, p. 103–106, https://doi.org/10.1130/G24003A.1.
D'Anastasio, E.D., De Martini, P.M., Sevaggi, G., Pantosti, D., Marchioni, A., and Maseroli, R., 2006, Short-term vertical velocity field in the Apennines (Italy) revealed by geodetic levelling data: Tectonophysics, v. 418, p. 219–234, https://doi.org/10.1016/j.tecto.2006.02.008.
Dell'Agnese, A., Brardinoni, F., Toro, M., Mao, L., Engel, M., and Comiti, F., 2015, Bedload transport in a formerly glaciated mountain catchment constrained by particle tracking: Earth Surface Dynamics, v. 3, p. 527–542, https://doi.org/10.5194/esurf-3-527-2015.
Dietrich, W.E., Dunne, T., Humphrey, N., and Reid, L., 1982, Construction of sediment budgets for drainage basins, *in* Swanson, F.J., Janda, R.J., Dunne, T., and Swanston, D.N., eds., Sediment Budgets and Routing in Forested Drainage Basins: Portland, Oregon, Pacific North-west Forest and Range Experiment Station: U.S. Department of Agriculture, Forest Service General Technical Report PNW-141, p. 2–23.
Dietrich, W.E., Kirchner, J.W., Ikeda, H., and Iseya, F., 1989, Sediment supply and the development of the coarse surface layer in gravel-bedded rivers: Nature, v. 340, p. 215–217, https://doi.org/10.1038/340215a0.
Dunne, T., Mertes, L.A.K., Meade, R.H., Richey, J.E., and Forsberg, B.R., 1998, Exchanges of sediment between the flood plain and channel of the Amazon River in Brazil: Geological Society of America Bulletin, v. 110, p. 450–467, https://doi.org/10.1130/0016-7606(1998)110<0450:EOSBTF>2.3.CO;2.
Finnegan, N.J., and Balco, G., 2013, Sediment supply, base level, braiding, and bedrock river terrace formation: Arroyo Seco, California, USA: Geological Society of America Bulletin, v. 125, p. 1114–1124, https://doi.org/10.1130/B30727.1.
Finnegan, N.J., Sklar, L.S., and Fuller, T.K., 2007, Interplay of sediment supply, river incision, and channel morphology revealed by the transient evolution of an experimental bedrock channel: Journal of Geophysical Research: Earth Surface, v. 112, no. F3, https://doi.org/10.1029/2006JF000569.
Franz, G., Leitao, P., Pinto, L., Jauch, E., Fernandes, L., and Neves, R., 2017, Development and validation of a morphological model for multiple sediment classes: International Journal of Sediment Research, v. 32, no. 4, p. 585–596, https://doi.org/10.1016/j.ijsrc.2017.05.002.
Fryirs, K.A., Wheaton, J.M., and Brierley, G.J., 2016, An approach for measuring confinement and assessing the influence of valley setting on river forms and processes: Earth Surface Processes and Landforms, v. 41, p. 701–710, https://doi.org/10.1002/esp.3893.
Fuller, T.K., Perg, L.A., Willenbring, J.K., and Lepper, K., 2009, Field evidence for climate-driven changes in sediment supply leading to strath terrace formation: Geology, v. 37, p. 467–470, https://doi.org/10.1130/G25487A.1.
Gallen, S.F., Wegman, K.W., Frankel, K.L., Hughes, S., Lewis, R.Q., Lyons, N., Paris, P., Ross, K., Bauer, J.B., and Witt, A.C., 2011, Hillslope response to knickpoint migration in the Southern Appalachians: Implications for the evolution of post-orogenic landscapes: Earth Surface Processes and Landforms, v. 36, p. 1254–1267, https://doi.org/10.1002/esp.2150.
Gilbert, G.K., 1877, Geology of the Henry Mountains: Washington, D.C., U.S. Government Printing Office, 170 p., https://doi.org/10.5962/bhl.title.51652.
Gilbert, G.K., 1914, The Transportation of Debris by Running Water: U.S. Geological Survey Professional Paper 86, 263 p., https://doi.org/10.5962/bhl.title.45583.
Glade, R.C., Shobe, C.M., Anderson, R.S., and Tucker, G.E., 2019, Canyon shape and erosion dynamics governed by channel-hillslope feedbacks: Geology, v. 47, p. 650–654, https://doi.org/10.1130/G46219.1.
Golly, A., Turowski, J.M., Badoux, A., and Hovius, N., 2017, Controls and feedbacks in the coupling of mountain channels and hillslopes: Geology, v. 45, p. 307–310, https://doi.org/10.1130/G38831.1.
Grant, G.E., and Swanson, F.J., 1995, Morphology and processes of valley floors in mountain streams, western Cascades, Oregon: American Geophysical Union Monograph 89, p. 83–101, https://doi.org/10.1029/GM089p0083.
Green, K.C., Brardinoni, F., and Alila, Y., 2013, Channel morphology and bed-load yield in fluvial, formerly-glaciated headwater streams of the Columbia Mountains, Canada: Geomorphology, v. 188, p. 96–109, https://doi.org/10.1016/j.geomorph.2012.05.004.
Gurnell, A.M., 1997, Channel change of the river Dee meanders, 1946–1992, from the analysis of air photographs: Regulated Rivers, v. 13, p. 13–26, https://doi.org/10.1002/(SICI)1099-1646(199701)13:1<13::AID-RRR420>3.0.CO;2-W.
Hassan, M.A., Bird, S., Reid, D., Ferrer-Boix, C., Hogan, D., Brardinoni, F., and Chartrand, S., 2019, Variable hillslope-channel coupling and channel characteristics of forested mountain streams in glaciated landscapes: Earth Surface Processes and Landforms, v. 44, p. 736–751, https://doi.org/10.1002/esp.4527.
Hayakawa, Y.S., and Matsukura, Y., 2003, Recession rates of waterfalls in Boso Peninsula, Japan, and a predictive equation: Earth Surface Processes and Landforms, v. 28, p. 675–684, https://doi.org/10.1002/esp.519.
Hickey, R., Smith, A., and Jankowski, P., 1994, Slope length calculations from a DEM within Arc/Info grid: Computers, Environment and Urban Systems, v. 18, no. 5, p. 365–380, https://doi.org/10.1016/0198-9715(94)90017-5.
Hughes, M.L., McDowell, P.F., and Marcus, W.A., 2006, Accuracy assessment of georectified aerial photographs: Implications for measuring lateral channel movement in a GIS: Geomorphology, v. 74, p. 1–16, https://doi.org/10.1016/j.geomorph.2005.07.001.
IDROSER (Idrorisorse per lo sviluppo dell'Emilia Romagna), 1981, Piano progettuale per la difesa della costa adriatica Emiliano-Romagnola: Bologna, Idroser, il Trasporto Solido Fluviale nei Bacini Tributari dell'Adriatico, v. 4, 429 p.
James, L.A., 2004, Tailings fans and valley-spur cutoffs created by hydraulic mining: Earth Surface Processes and Landforms, v. 29, p. 869–882, https://doi.org/10.1002/esp.1075.
Janbu, N., Bjerrum, L., and Kjaernsli, B., 1956, Veiledning Ved Losing av Fandamenteringsoppgaver [Soil Mechanics Applied to Some Engineering Problems; in Norwegian with English summary]: Norwegian Geotechnical Institute Publication 16.
Jansen, J.D., Fabel, D., Bishop, P., Xu, S., Schnabel, C., and Codilean, A.T., 2011, Does decreasing paraglacial sediment supply slow knickpoint retreat?: Geology, v. 39, p. 543–546, https://doi.org/10.1130/G32018.1.
Johnson, K.N., and Finnegan, N.J., 2015, A lithologic control on active meandering in bedrock channels: Geological Society of America Bulletin, v. 127, p. 1766–1776, https://doi.org/10.1130/B31184.1.
Kasprak, A., Wheaton, J.M., Ashmore, P.E., Hensleigh, J.W., and Peirce, S., 2015, The relationship between particle travel distance and channel morphology: Results from physical models of braided rivers: Journal of Geophysical Research: Earth Surface, v. 120, no. 1, p. 55–74, https://doi.org/10.1002/2014JF003310.
Keesstra, S.D., van Huissteden, J., Vandenberghe, J., Van Dam, O., de Gier, J., and Pleizer, I.D., 2005, Evolution of the morphology of the river Dragonja (SW Slovenia) due to land-use changes: Geomorphology, v. 69, p. 191–207, https://doi.org/10.1016/j.geomorph.2005.01.004.
Kelsey, H.M., Lamberson, R., and Madej, M.A., 1987, Stochastic model for the long-term transport of stored sediment in a river channel: Water Resources Research, v. 23, p. 1738–1750, https://doi.org/10.1029/WR023i009p01738.
Kuo, C.W., and Brierley, G.J., 2013, The influence of landscape configuration upon patterns of sediment storage in a highly connected river system: Geomorphology, v. 180–181, p. 255–266, https://doi.org/10.1016/j.geomorph.2012.10.015.
Lamb, M.P., and Fonstad, M.A., 2010, Rapid formation of a modern bedrock canyon by a single flood event: Nature

Geoscience, v. 3, no. 7, p. 477–481, https://doi.org/10.1038/ngeo894.

Lamb, M.P., Howard, A.D., Dietrich, W.E., and Peron, J.T., 2007, Formation of amphitheatre-headed valleys by waterfall erosion after large-scale slumping on Hawai'i: Geological Society of America Bulletin, v. 119, p. 805–822, https://doi.org/10.1130/B25986.1.

Lamb, M.P., Mackey, B.H., and Farley, K.A., 2014, Amphitheater-headed canyons formed by megaflooding at Malad Gorge, Idaho: Proceedings of the National Academy of Sciences of the United States of America, v. 111, no. 1, p. 57–62, https://doi.org/10.1073/pnas.1312251111.

Lamb, M.P., Finnegan, N.J., Scheingross, J.S., and Sklar, L.S., 2015, New insights into the mechanics of fluvial bedrock erosion through flume experiments and theory: Geomorphology, v. 244, p. 33–55, https://doi.org/10.1016/j.geomorph.2015.03.003.

Langendoen, E.J., and Alonso, C.V., 2008, Modeling the evolution of incised streams: I. Model formulation and validation of flow and streambed evolution components: Journal of Hydraulic Engineering, v. 134, no. 6, p. 749–762, https://doi.org/10.1061/(ASCE)0733-9429(2008)134:6(749).

Langendoen, E.J., and Simon, A., 2008, Modeling the evolution of incised streams: II. Streambank erosion: Journal of Hydraulic Engineering, v. 134, no. 7, p. 905–915, https://doi.org/10.1061/(ASCE)0733-9429(2008)134:7(905).

Lapotre, M.G.A., Lamb, M.P., and Williams, R.M.E., 2016, Canyon formation constraints on the discharge of catastrophic outburst floods of Earth and Mars: Journal of Geophysical Research: Planets, v. 121, p. 1232–1263, https://doi.org/10.1002/2016JE005061.

Leopold, L.B., and Bull, W.B., 1979, Base level, aggradation, and grade: Proceedings of the American Philosophical Society, v. 123, no. 2, p. 168–202.

Liébault, F., and Piégay, H., 2001, Assessment of channel changes due to long-term bedload supply decrease, Roubion River, France: Geomorphology, v. 36, p. 167–186, https://doi.org/10.1016/S0169-555X(00)00044-1.

Liébault, F., and Piégay, H., 2002, Causes of 20th century channel narrowing in mountain and piedmont rivers of Southeastern France: Earth Surface Processes and Landforms, v. 27, p. 425–444, https://doi.org/10.1002/esp.328.

Lindsay, J.B., and Ashmore, P.E., 2002, The effects of survey frequency on estimates of scour and fill in a braided river model: Earth Surface Processes and Landforms, v. 27, p. 27–43, https://doi.org/10.1002/esp.282.

Lisle, T.E., 1982, Effects of aggradation and degradation on riffle-pool morphology in natural gravel channels, northwestern California: Water Resources Research, v. 18, no. 6, p. 1643–1651, https://doi.org/10.1029/WR018i006p01643.

Lisle, T.E., and Church, M., 2002, Sediment transport-storage relations for degrading, gravel bed channels: Water Resources Research, v. 38, no. 11, p. 1-1–1-14, https://doi.org/10.1029/2001WR001086.

Llena, M., Vericat, D., Martínez-Casasnovas, J.A., and Smith, M.W., 2020, Geomorphic adjustments to multi-scale disturbances in a mountain river: A century of observations: Catena, v. 192, https://doi.org/10.1016/j.catena.2020.104584.

Llena, M., Simonelli, T., and Brardinoni, F., 2022, Rapid formation of a bedrock canyon following gravel mining in the Marecchia River, Northern Apennines: Abstract presented at European Geosciences Union General Assembly 2022, Vienna, Austria, 23–27 May, https://doi.org/10.5194/egusphere-egu22-6894.

Mackin, J.H., 1948, Concept of the Gravel River: Geological Society of America Bulletin, v. 59, p. 463–512, https://doi.org/10.1130/0016-7606(1948)59[463:COTGR]2.0.CO;2.

Madej, M.A., 2001, Development of channel organization and roughness following sediment pulses in single-thread, gravel bed rivers: Water Resources Research, v. 37, no. 8, p. 2259–2272, https://doi.org/10.1029/2001WR000229.

Milliman, J.D., and Farnsworth, K.L., 2011, River Discharge to the Coastal Ocean: A Global Synthesis: Cambridge University Press, https://doi.org/10.1017/CBO9780511781247.

Milliman, J.D., and Syvitski, J.P., 1992, Geomorphic/tectonic control of sediment discharge to the ocean: The importance of small mountainous rivers: The Journal of Geology, v. 100, no. 5, p. 525–544, https://doi.org/10.1086/629606.

Montgomery, D.R., and Buffington, J.M., 1997, Channel-reach morphology in mountain drainage basins: Geological Society of America Bulletin, v. 109, p. 596–611, https://doi.org/10.1130/0016-7606(1997)109<0596:CRMIMD>2.3.CO;2.

Mudd, S.M., and Furbish, D.J., 2007, Responses of soil-mantled hillslopes to transient channel incision rates: Journal of Geophysical Research: Earth Surface, v. 112, no. F3, https://doi.org/10.1029/2006JF000516.

O'Brien, G.R., Wheaton, J.M., Fryirs, K., Macfarlane, W.W., Brierley, G., Whitehead, K., Gilbert, J., and Volk, C., 2019, Mapping valley bottom confinement at the network scale: Earth Surface Processes and Landforms, v. 44, p. 1828–1845, https://doi.org/10.1002/esp.4615.

Osman, A M., and Thorne, C.R., 1988, Riverbank stability analysis. I: Theory: Journal of Hydraulic Engineering, v. 114, no. 2, p. 134–150, https://doi.org/10.1061/(ASCE)0733-9429(1988)114:2(134).

Parker, C., Simon, A., and Thorne, C.R., 2008, The effects of variability in bank material properties on riverbank stability: Goodwin Creek, Mississippi: Geomorphology, v. 101, p. 533–543, https://doi.org/10.1016/j.geomorph.2008.02.007.

Reid, L.M., and Dunne, T., 1996, Rapid Evaluation of Sediment Budgets: Reiskirchen, Germany, Catena Verlag, 164 p.

Reusser, L.J., Bierman, P.R., Pavich, M.J., Zen, E., Larsen, J., and Finkel, R., 2004, Rapid late Pleistocene incision of Atlantic passive-margin river gorges: Science, v. 305, no. 5683, p. 499–502, https://doi.org/10.1126/science.1097780.

Rinaldi, M., and Darby, S.E., 2008, Modelling river-bank-erosion processes and mass failure mechanisms: Progress towards fully coupled simulations, *in* Habersack, H., Piégay, H., and Rinaldi, M., eds., Gravel-Bed Rivers VI: From Process Understanding to River Restoration: Elsevier, p. 213–239.

Sanders, D., Wischounig, L., Gruber, A., and Ostermann, M., 2014, Inner gorge-slot canyon system produced by repeated stream incision (Eastern Alps): Significance for development of bedrock canyons: Geomorphology, v. 214, p. 465–484, https://doi.org/10.1016/j.geomorph.2014.03.007.

Schanz, S.A., Montgomery, D.R., Collins, B.D., and Duvall, A.R., 2018, Multiple paths to straths: A review and reassessment of terrace genesis: Geomorphology, v. 312, p. 12–23, https://doi.org/10.1016/j.geomorph.2018.03.028.

Schanz, S.A., Montgomery, D.R., and Collins, B.D., 2019, Anthropogenic strath terrace formation caused by reduced sediment retention: Proceedings of the National Academy of Sciences of the United States of America, v. 116, no. 18, p. 8734–8739, https://doi.org/10.1073/pnas.1814627116.

Scheingross, J.S., and Lamb, M.P., 2017, A mechanistic model of waterfall plunge pool erosion into bedrock: Journal of Geophysical Research: Earth Surface, v. 122, p. 2079–2104, https://doi.org/10.1002/2017JF004195.

Scorpio, V., and Piegay, H., 2021, Is afforestation a driver of change in Italian rivers within the Anthropocene era?: Catena, v. 198, https://doi.org/10.1016/j.catena.2020.105031.

Scorpio, V., Aucelli, P.P.C., Giano, S.I., Pisano, L., Robustelli, G., Rosskopf, C.M., and Schiattarella, M., 2015, River channel adjustments in Southern Italy over the past 150 years and implications for channel recovery: Geomorphology, v. 251, p. 77–90, https://doi.org/10.1016/j.geomorph.2015.07.008.

Shobe, C.M., Tucker, G.E., and Anderson, R.S., 2016, Hillslope-derived blocks retard river incision: Geophysical Research Letters, v. 43, no. 10, p. 5070–5078, https://doi.org/10.1002/2016GL069262.

Simon, A., and Rinaldi, M., 2006, Disturbance, stream incision, and channel evolution: The roles of excess transport capacity and boundary materials in controlling channel response: Geomorphology, v. 79, p. 361–383, https://doi.org/10.1016/j.geomorph.2006.06.037.

Simon, A., Rinaldi, M., and Hadish, G., 1996, Channel evolution in the loess area of the Midwestern United States: Proceedings of Sixth Federal Interagency Sedimentation Conference, v. 3, p. 86–93.

Simon, A., Curini, A., Darby, S.E., and Langendoen, E.J., 2000, Bank and near-bank processes in an incised channel: Geomorphology, v. 35, p. 193–217, https://doi.org/10.1016/S0169-555X(00)00036-2.

Sklar, L., and Dietrich, W.E., 1998, River longitudinal profiles and bedrock incision models: Stream power and the influence of sediment supply, *in* Tinkler, K.J., and Wohl, E.E., eds., Rivers Over Rock: Fluvial Processes in Bedrock Channels: American Geophysical Union, Geophysical Monograph 107, p. 237–260, https://doi.org/10.1029/GM107p0237.

Sklar, L.S., and Dietrich, W.E., 2004, A mechanistic model for river incision into bedrock by saltating bed load: Water Resources Research, v. 40, no. 6, https://doi.org/10.1029/2003WR002496.

Slaymaker, O., 2003, The sediment budget as conceptual framework and management tool: Hydrobiologia, v. 494, p. 71–82, https://doi.org/10.1023/A:1025437509525.

Snyder, N.P., and Whipple, K.X., 2003, Importance of a stochastic distribution of floods and erosion thresholds in the bedrock river incision problem: Journal of Geophysical Research: Solid Earth, v. 108, no. B2, https://doi.org/10.1029/2001JB001655.

Stock, J.D., Montgomery, D.R., Collins, B.D., Dietrich, W.E., and Sklar, L., 2005, Field measurements of incision rates following bedrock exposure: Implications for process controls on the long profiles of valleys cut by rivers and debris flows: Geological Society of America Bulletin, v. 117, p. 174–194, https://doi.org/10.1130/B25560.1.

Surian, N., and Rinaldi, M., 2003, Morphological response to river engineering and management in alluvial channels in Italy: Geomorphology, v. 50, p. 307–326, https://doi.org/10.1016/S0169-555X(02)00219-2.

Surian, N., Rinaldi, M., Pellegrini, L., Audisio, C., Maraga, F., Teruggi, L., Turitto, O., and Ziliani, L., 2009, Channel adjustments in northern and central Italy over the last 200 years, *in* James, L.A., Rathburn, S.L., and Whittecar, G.R., eds., Management and Restoration of Fluvial Systems with Broad Historical Changes and Human Impacts: Geological Society of America Special Paper 451, p. 83–95, https://doi.org/10.1130/2009.2451(05).

Thompson, D., and Wohl, E., 1998, Flume experimentation and simulation of bedrock channel processes, *in* Tinkler, K.J., and Wohl, eds., Rivers over Rock: Fluvial Processes in Bedrock Channels: American Geophysical Union, Geophysical Monograph 107, p. 279–296, https://doi.org/10.1029/GM107p0279.

Tinterri, R., and Muzzi-Magalhaes, P., 2011, Synsedimentary structural control on foredeep turbidites: An example from Miocene Marnoso-arenacea Formation, Northern Apennines, Italy: Marine and Petroleum Geology, v. 28, p. 629–657, https://doi.org/10.1016/j.marpetgeo.2010.07.007.

Toone, J., Rice, S.P., and Piégay, H., 2014, Spatial discontinuity and temporal evolution of channel morphology along a mixed bedrock-alluvial river, upper Drôme River, southeast France: Contingent responses to external and internal controls: Geomorphology, v. 205, p. 5–16, https://doi.org/10.1016/j.geomorph.2012.05.033.

Trimble, S.W., 1983, A sediment budget for Coon Creek basin in the Driftless area, Wisconsin, 1853–1977: American Journal of Science, v. 283, no. 5, p. 454–474, https://doi.org/10.2475/ajs.283.5.454.

Venditti, J.G., Dietrich, W.E., Nelson, P.A., Wydzga, M.A., Fadde, J., and Sklar, L., 2010, Effect of sediment pulse grain size on sediment transport rates and bed mobility in gravel bed rivers: Journal of Geophysical Research: Earth Surface, v. 115, no. F3, https://doi.org/10.1029/2009JF001418.

Vericat, D., Wheaton, J.M., and Brasington, J., 2017, Revisiting the morphological approach: Opportunities and challenges with repeat high-resolution topography, *in*

Tsutsumi, D., and Laronne, J.B., eds., Gravel-Bed Rivers: Process and Disasters: Wiley, p. 121–158, https://doi.org/10.1002/9781118971437.ch5.

Wegmann, K.W., and Pazzaglia, F.J., 2002, Holocene strath terraces, climate change, and active tectonics; the Clearwater River basin, Olympic Peninsula, Washington State: Geological Society of America Bulletin, v. 114, p. 731–744, https://doi.org/10.1130/0016-7606(2002)114<0731:HSTCCA>2.0.CO;2.

Wheaton, J.M., Brasington, J., Darby, S.E., and Sear, D.A., 2010, Accounting for uncertainty in DEMs from repeat topographic surveys: Improved sediment budgets: Earth Surface Processes and Landforms, v. 35, no. 2, p. 136–156.

Whipple, K.X., 2001, Fluvial landscape response time: How plausible is steady-state denudation?: American Journal of Science, v. 301, p. 313–325, https://doi.org/10.2475/ajs.301.4-5.313.

Whipple, K.X., and Tucker, G., 2002, Implications of sediment-flux dependent river incision models for landscape evolution: Journal of Geophysical Research: Solid Earth, v. 107, p. ETG 3-1–ETG 3-20, https://doi.org/10.1029/2000JB000044.

Whiting, P.J., Matisoff, G., Fornes, W., and Soster, F.M., 2005, Suspended sediment sources and transport distances in the Yellowstone River basin: Geological Society of America Bulletin, v. 117, p. 515–529, https://doi.org/10.1130/B25623.1.

Whittaker, A.C., and Boulton, S.J., 2012, Tectonic and climatic controls on knickpoint retreat rates and landscape response times: Journal of Geophysical Research: Earth Surface, v. 117, https://doi.org/10.1029/2011JF002157.

Yanites, B.J., 2018, The dynamics of channel slope, width, and sediment in actively eroding bedrock river systems: Journal of Geophysical Research: Earth Surface, v. 123, p. 1504–1527, https://doi.org/10.1029/2017JF004405.

Ziliani, L., and Surian, N., 2012, Evolutionary trajectory of channel morphology and controlling factors in a large gravel-bed river: Geomorphology, v. 173–174, p. 104–117, https://doi.org/10.1016/j.geomorph.2012.06.001.

Science Editor: Brad Singer
Associate Editor: John Jansen

Manuscript Received 16 August 2022
Revised Manuscript Received 2 March 2023
Manuscript Accepted 3 April 2023

Printed in the USA